Contrib Mineral Petrol (2002) 142: 543–563
DOI 10.1007/s004100100309

Ulrike Troitzsch · David J. Ellis

Thermodynamic properties and stability of AlF-bearing titanite $CaTiOSiO_4$–$Ca\text{-}AlFSiO_4$

Received: 16 August 2001 / Accepted: 27 August 2001 / Published online: 23 October 2001

Abstract Calorimetric and experimental data on AlF-bearing titanite are presented that yield thermodynamic properties of $CaAlFSiO_4$, as well as activity-composition relations of binary titanite $CaTiOSiO_4$–$CaAlFSiO_4$. The heat capacity of synthetic $CaAlFSiO_4$ was measured with differential scanning calorimetry between 170 and 850 K:

$$C_P = 689.96 - 0.38647T + 2911300T^{-2} - 8356.1T^{-0.5} + 0.00016179T^2$$

Based on low-temperature heat capacity calculations with lattice vibrational theory (Debye model), the calorimetric entropy of $CaAlFSiO_4$ can be expected to lie between 104.7 and 118.1 J mol^{-1} K^{-1}. The temperature of the $P2_1/a$ to $A2/a$ phase change was determined calorimetrically for a titanite with $X_{Al} = 0.09$ ($T_{transition} = 390$ K). The decrease of the transition temperature at a rate of about 11 K per mol% $CaAlFSiO_4$ is in good agreement with previous TEM investigations. The displacement of the reaction anorthite + fluorite = $CaAlFSiO_4$ in the presence of $CaTiOSiO_4$ was studied with high P–T experiments. Titanite behaves as a non-ideal, symmetrical solid-solution. The thermodynamic properties of $CaAlFSiO_4$ consistent with a multi-site mixing model are:

Enthalpy of formation (elements) d_fH^0	$= -2740.8 \pm 3.0$ kJmol^{-1}
Standard state entropy S^0	$= 104.9 \pm 1.1$ Jmol^{-1}K^{-1}
Margules parameter $[W_H - TW_S]$	$= 13.6 \pm 0.4$ Jmol^{-1}

The pressure dependence of the Margules parameter (W_V) was determined from the excess volume of mixing based on XRD measurements (214 ± 18 J mol^{-1} kbar^{-1}), as well as refined from the piston-cylinder experimental results (198 ± 114 J mol^{-1} kbar^{-1}), demonstrating consistency between crystal structure data and thermodynamic properties. The stability of AlF-bearing titanite $Ca(Ti,Al)(O,F)SiO_4$ was investigated by thermodynamic modelling in the system Ca–Al–Si–Ti–O–F–H–C and subsystems. The petrogenetic grids are in good agreement with natural mineral assemblages, in that very Al-rich titanite ($X_{Al} > 0.65 \pm 0.15$) is generally absent because it is either unstable with respect to other phases, or its stability field lies outside the P–T conditions realised on Earth. The grids explain both the predominant occurrence of natural Al-rich titanite at high metamorphic grade such as eclogite facies conditions, as well as its scarcity in blueschist facies rocks. Wide spacing of the Al-isopleths for titanite of many high-grade assemblages prevents their use as geobarometers or thermometers. The instability of end-member $CaAlFSiO_4$ with respect to other phases in most assemblages modelled here is consistent with the hypothesis that the presence of structural stresses in the crystal lattice of $CaAlFSiO_4$ influences its thermodynamic stability. The titanite structure is not well suited to accommodate Al and F instead of Ti and O, causing the relatively high Gibbs free energy of $CaAlFSiO_4$, manifested in its standard state properties. Thus, the increasing amount of $CaAlFSiO_4$ along the binary join is the reason why titanite with $X_{Al} > 0.65 \pm 0.15$ becomes unstable in most petrogenetic grids presented here. The compositional limit of natural titanite ($X_{Al} \approx 0.54$) probably reflects the point beyond which the less stable end member begins to dominate the solid-solution, affecting both crystal structure and thermodynamic stability.

U. Troitzsch (✉) · D.J. Ellis
Department of Geology,
Australian National University,
Canberra, ACT 0200, Australia
E-mail: ulrike@geology.anu.edu.au

Editorial responsibility: I. Parsons

Introduction

Titanite ($CaTiOSiO_4$) is a common accessory phase in a range of igneous, metamorphic, and some sedimentary rocks. The widespread occurrence of titanite

throughout different geochemical environments and petrogenetic conditions is caused by the large number of other elements that can be substituted into its crystal structure (e.g. Sahama 1946; Oberti et al. 1991). Numerous studies based on natural assemblages, experiments and thermodynamic modelling proposed that titanite is a potential indicator for a range of metamorphic conditions (Kowallis et al. 1997), such as pressure and temperature (Essene and Bohlen 1985; Manning and Bohlen 1991; Mukhopadhyay et al. 1992; Ghent and Stout 1994), fluid composition (Hunt and Kerrick 1977; Valley and Essene 1980; Jacobs and Kerrick 1981; Itaya et al. 1985) and oxygen fugacity (Spear 1981; Wones 1989). Its U–Pb content opens the exciting possibility to date the above metamorphic conditions (Frost et al. 2001). Understanding the stability of titanite in igneous and metamorphic rocks is important because it might play a dominant role in shaping their rare earth element patterns (Hellman and Green 1979, Green and Pearson 1986; Paterson and Stephens 1992; Dawson et al. 1994; Tribuzio et al. 1996). Moreover, the presence or absence of titanite in felsic igneous rocks could be used as an indicator for F contents of magmas (Price et al. 1999).

Because titanite commonly occurs in solid-solution with other end members, it is crucial to understand the mixing behaviour, and activity-composition relations of the most important end members. Although the thermodynamic data of the titanite end member ($CaTiOSiO_4$) are known, activity-composition relations of titanite solid-solution had never been determined, so that previous studies assumed either ideal mixing behaviour (Ghent and Stout 1994) or titanite to be pure $CaTiOSiO_4$ (Mukhopadhyay et al. 1992). Throughout the present paper 'titanite' stands for the phase titanite, thus including solid-solution, whereas pure titanite is referred to as 'end member titanite' or '$CaTiOSiO_4$'.

In the present study we investigated experimentally the activity–composition relations of Al-bearing titanite along the binary join $CaTiOSiO_4$–$CaAlFSiO_4$, represented by the coupled substitution

$$Ti^{4+}+O^{2-}=Al^{3+}+F^{-} \quad (1)$$

The end member $CaAlFSiO_4$ was chosen for several reasons. First, Al is one of the most common and abundant substituents for Ti in natural titanite, and thus most important for thermodynamic modelling of natural assemblages. Second, among the two main Al end members that occur in natural titanite, i.e. $CaAlOHSiO_4$ and $CaAlFSiO_4$, the latter always dominates in the most Al-rich titanites, but never exceeds 54 mol% (Franz and Spear 1985, Markl and Piazolo 1999). The reasons for this compositional limit were the subject of much discussion (Smith 1981, Oberti et al. 1991). Crystal structure investigations along the join TiO–AlF indicated that, although complete solid-solution is observed, the titanite structure is not well suited to accommodate $X_{Al} > 0.5$ (Troitzsch et al. 1999). We examine whether these crystal structural problems are reflected in the thermodynamics of this system, for example as an activity anomaly at this composition. There has been no previous attempt to equilibrate more AlF-rich titanite in a mineralogically buffered phase assemblage. Although Smith (1981) determined qualitatively the dependence of the AlF content in titanite on pressure and temperature with experiments, the equilibrated phase assemblage contained melt and, thus, was not mineralogically buffered, preventing a thorough thermodynamic interpretation of the results. Note, however, the recent study by Tropper et al. (1999, 2000) discussed below. Third, the unit-cell volume of titanite along the binary join TiO–AlF has recently been determined (Troitzsch and Ellis 1999; Troitzsch et al. 1999), permitting accurate thermodynamic calculations with this end member. Fourth, the Al content of titanite is pressure- and temperature-dependent, and thus of special interest for geothermobarometry (Smith 1981; Enami et al. 1993; Franz and Spear 1985).

The potential of Al-bearing titanite in geobarometry has long been recognised (Smith 1980; 1981). Many previous studies of natural (e.g. Franz and Spear 1985; Krogh et al. 1990; Enami et al. 1993; Carswell et al. 1996) and synthetic Al-rich titanite (Smith 1981) have suggested a strong pressure and mild temperature dependence of the Al content in titanite. However, the PTX relationship was never quantified for any assemblage, mainly because of the strong dependence of the system on fluorine, which, until more recently, was difficult to analyse quantitatively with standard equipment.

In the first part of this study we investigated, with differential scanning calorimetry, the heat capacity of synthetic $CaAlFSiO_4$ required for the subsequent interpretation of high P–T-experiments. Secondly, the $P2_1/a$ to $A2/a$ phase transition temperature of a synthetic titanite with $X_{AlF}=0.09$ was determined calorimetrically to improve the resolution of the $CaTiOSiO_4$–$CaAlFSiO_4$ phase diagram. Thirdly, a series of piston-cylinder experiments was carried out in the system Ca–Ti–Al–Si–O–F, determining the displacement of the reaction

$$\begin{array}{l} 0.5CaAl_2Si_2O_8 + 0.5CaF_2 = CaAlFSiO_4 \\ \quad \text{Anorthite} \quad + \text{fluorite} \ = \text{AlF titanite} \end{array} \quad (2)$$

in the presence of $CaTiOSiO_4$. This gave the activity–composition relationship of titanite solid-solution, and the standard state entropy and enthalpy of formation of $CaAlFSiO_4$. These thermodynamic data were then used to investigate the stability of AlF-rich titanite.

Differential scanning calorimetry details

The heat capacity of $CaAlFSiO_4$ was determined using the synthetic sample G-297 of Troitzsch and Ellis (1999). This sample contains small amounts of fluorine-rich zoisite, fluorite, and trace

kyanite. As the bulk composition of the sample should be that of $CaAlFSiO_4$, and heat capacities of different phases of equivalent composition are similar, the impurities cause only small errors compared with those inherent in the calorimetric equipment and experimental method. The temperature of the $P2_1/a$ to $A2/a$ phase transition was determined for a titanite with $X_{Al} = 0.094 \pm 0.008$ (sample AlF09) synthesized at 1,000 °C and 10 kbar from synthetic wollastonite, rutile, anorthite and fluorite (details as in Troitzsch et al. 1999). Sample AlF09 was investigated with SEM and XRD to ensure that only homogeneous titanite was present.

All measurements were carried out with a differential scanning calorimeter DSC 2920 (TA Instruments). Temperature calibrations performed on phase transitions of indium, tin, zinc and $C_{10}H_8$ indicate an accuracy of ±1.5° over the temperature range of 353 to 670 K. Non-hermetically sealing aluminium pans were used. Although the calorimetric precision of the instrument is given as 1% by the manufacturer, multiple scans indicated that heat capacities were reproduced to within 2%. Problems encountered during a different set of heat capacity measurements using this calorimeter are described in Troitzsch (2000) who recommended that the heat capacity of $CaAlFSiO_4$ be confirmed with a different instrument.

All samples were finely ground in acetone in an agate mortar, and dried. Between 30 and 50 mg of powder was filled into the pans. The lids were inverted in order to compact the powder firmly in the pan, which improves the contact of the sample with the pan bottom and thus with the thermocouple, and facilitates heat transfer in the sample. This was especially important for the transition temperature measurement because it significantly smoothed the trace, probably by limiting movement of grains within the sample during heating. The extremely weak signal of the phase transition would otherwise not have been discerned from background noise. The $CaAlFSiO_4$ sample was annealed above 800 K for about 30 min to avoid strain-release and recrystallization effects during the run. A sapphire standard was run immediately before each $CaAlFSiO_4$ sample. Only the heat flow was determined for sample AlF09. All standard and sample runs were performed at a heating rate of 20° min^{-1}, from 170 to 850 K. Two scans of $CaAlFSiO_4$ were performed, the mean of which was taken as the final value.

Piston-cylinder experiments details

Eighteen polybaric runs (1,000 °C) and two sets of polythermal runs (four at 7 kbar, five at 10 kbar) produced AlF-bearing titanite in the assemblage titanite–anorthite–fluorite (Table 1). The starting mixes of binary titanite composition ($X_{Al} = 0.60$ to $X_{Al} = 0.96$) were composed of synthetic anorthite, wollastonite, fluorite (Specpure), and TiO_2 (Degussa). The synthesis of anorthite and wollastonite from glass was described in Troitzsch and Ellis (1999) and Troitzsch et al. (1999). 2-mm diameter $Ag_{0.75}Pd_{0.25}$ capsules were filled with the starting powder, dried for at least 2 h at 110 °C, and then welded shut. Experimental procedure was as described in Troitzsch et al. (1999). An error of ±0.2 kbar of all pressure readings, and ±5 °C with respect to temperature, was used in the curve fitting procedure.

One set of reversal experiments was carried out at 10 kbar, re-equilibrating run products of samples G-395 and G-398, previously run at 12 and 8 kbar, respectively (Table 1). Each sample was reground, filled in a 2-mm diameter $Ag_{0.75}Pd_{0.25}$ capsule, dried and welded shut. Both capsules were then placed next to each other in the same pressure assembly and run in one experiment to ensure identical pressure and temperature conditions. The second set of reversals consisted of samples G-407 and G-411, formerly equilibrated at 17 and 14 kbar, which were re-run at 15.5 kbar.

The run products were investigated with reflected light microscopy, X-ray diffraction and scanning electron microscopy. Although in high-temperature runs (> 900 °C) the grain-size of the products (< 10 μm) enabled the determination of the titanite

Table 1 Run conditions and results of piston-cylinder experiments. *An* Anorthite; *Fluo* fluorite; *Gro* grossular; *Ttn* titanite; *Zoi* zoisite

Exp. no.	T (°C)	P (kbar)	t[a] (h)	X_{Al} Mix	Run products	X_{Al} Ttn	SD X_{Al}
G-391	1,000	5	70	0.60	Ttn An Fluo	0.282	0.007
G-396	1,000	5	71	0.60	Ttn An Fluo	0.282[b]	0.004
G-392	1,000	6	70	0.60	Ttn An Fluo	0.290[b]	0.004
G-444	800	7	504	0.60	Ttn An Fluo	0.393[b]	0.004
G-416	850	7	192	0.80	Ttn An Fluo	0.371[b]	0.004
G-422	950	7	72	0.60	Ttn An Fluo	0.330[b]	0.004
G-402	1,000	7	58	0.60	Ttn An Fluo	0.309[b]	0.004
G-398	1,000	8	50	0.60	Ttn An Fluo	0.340	0.011
G-389	1,000	9	70	0.60	Ttn An Fluo	0.367	0.005
G-382	800	10	480	0.60	Ttn An Fluo Gro[c]	0.519[b]	0.004
G-383	850	10	480	0.60	Ttn An Fluo	0.471	0.005
G-409	900	10	71	0.60	Ttn An Fluo	0.460[b]	0.004
G-404	950	10	71	0.60	Ttn An Fluo	0.417	0.014
G-400	1,000	10	50	0.60	Ttn An Fluo	0.394	0.012
G-388	1,000	11	70	0.60	Ttn An Fluo	0.422	0.009
G-397	1,000	11	71	0.60	Ttn An Fluo	0.427	0.019
G-395	1,000	12	36	0.60	Ttn An Fluo	0.464	0.016
G-386	1,000	13	68	0.60	Ttn An Fluo	0.487	0.013
G-411	1,000	14	44	0.84	Ttn An Fluo	0.563	0.014
G-413	1,000	15	79	0.84	Ttn An Fluo Zoi[c]	0.605	0.012
G-412	1,000	15.5	44	0.84	Ttn An Fluo	0.612	0.011
G-403	1,000	16	58	0.80	Ttn An Fluo Zoi[c]	0.632	0.014
G-407	1,000	17	51	0.84	Ttn An Fluo	0.679	0.013
G-418	1,000	20	67	0.96	Ttn An Fluo	0.816[b]	0.004
G-443	1,000	21	69	0.96	Ttn An Fluo Zoi[c]	0.914[b]	0.004

[a]Run duration
[b]Al content determined only with XRD via unit cell dimensions. Standard deviations of these values as given in the last column represent the estimated mean error of this method. All other values determined with SEM
[c]Trace amounts

composition with SEM, at lower temperatures the grain-size (< 2 μm) approached the analytical resolution limit of the SEM. Therefore, the AlF content of titanite in the latter as well as for some high temperature runs was determined indirectly via the unit-cell dimensions *a*, *b* and *c* of titanite, which were obtained from powder X-ray diffraction patterns using the Rietveld refinement computer program RIETAN (Izumi 1993; Kim and Izumi 1994). The change in unit-cell dimensions of synthetic titanite along the binary join $CaTiOSiO_4$–$CaAlFSiO_4$ are given in the Appendix, based on Troitzsch et al. (1999). The accuracy of this method was tested with several high temperature run products, which were coarse-grained and thus yielded reliable SEM analyses. Figure 1 shows that the AlF content obtained with XRD reproduces the mean of the SEM analyses of each sample with a precision of $X_{Al} \pm 0.004$, demonstrating the consistency of both methods, and the accuracy of the polynomial functions in the Appendix.

Quantitative analyses were obtained with a JEOL JSM-6400 scanning electron microscope with attached Si(Li) detector, Link ISIS EDS, at 15 kV and 1 nA. Analyses were calculated using a ZAF correction. Analysed elements were silicon (standard: SiO_2), titanium (TiO_2), aluminium and oxygen (albite), calcium (diopside) and fluorine (fluorite). The determination of the number of atoms per formula unit is based on three total cations (Franz and Spear 1985) instead of anion-based calculations because it avoids the propagation of large errors attached to the F-analyses (6%, as opposed to 1.0, 1.1, 0.6, 0.7 and 1.3% for oxygen, aluminium, silicon, calcium and titanium, respectively). A minimum of 10 titanite grains was analysed per sample. Apart from a slight Si deficiency of about 0.01 a.p.f.u., and a small surplus of Ca of about 0.02 a.p.f.u., the analyses suggest ideal occupation on all sites. Therefore, the amount of $CaAlFSiO_4$ was calculated as $X_{Al} = Al/(Al + Ti)$.

The interpretation of the experimental results [reaction (2)] was based on thermodynamic data of anorthite from Berman (1988), and fluorite from Robie and Hemingway (1995). Thermal expansion (Carmichael 1984) and isothermal compressibility of fluorite (Birch 1966) were transformed to suit the volume equation of Berman (1988) used in the regression. The molar volume of $CaAlFSiO_4$ was taken from Troitzsch et al. (1999). Expansion and compressibility of $CaAlFSiO_4$ were assumed to be identical to those of titanite, which were estimated based on the high pressure XRD data of Angel et al. (1999), and the high temperature studies of Taylor and Brown (1976) and Ghose et al. (1991). The pressure dependence of the Margules parameter of titanite ($W_V = 214.08 \pm 18$ J kbar^{-1}) was calculated from the excess volume of mixing determined by Troitzsch et al. (1999). Only data with $X_{Al} > 0.09$ were used, allowing a symmetrical fit to the data. The enthalpy of formation and entropy of $CaAlFSiO_4$, and the Margules parameter term (W_H–TW_S) were determined by free-energy minimization, fitting the experimental PTX_{Al} data to

$$\Delta G = 0 = \Delta H^0_{1,298} + \int_{298}^{T} C_P dT - T\Delta S^0_{1,298} - T\int_{298}^{T} \frac{C_P}{T} dT + \int_{1}^{P} \Delta V dP + RT \ln K \quad (3)$$

Two activity models were used. The multi-site mixing (MM) model assumes independent distribution of Al and F on each site, and is described by

$$RT \ln a^{Ttn}_{CaAlFSiO_4} = 2RT \ln X_{Al} + (W_H - TW_S + PW_V)(1 - X_{Al})^2 \quad (4)$$

Here, the Margules parameters are a combination of the Margules parameters for each site [$W_X = (W_X)_{Ti-Al} + (W_X)_{O-F}$]. The local charge balance (LCB) model is described by

$$RT \ln a^{Ttn}_{CaAlFSiO_4} = RT \ln X_{Al} + (W_H - TW_S + PW_V)(1 - X_{Al})^2 \quad (5)$$

Least squares regression of the experimental PTX_{Al} data-triplets was carried out with a BASIC program of Hugh O'Neill. This program performs a Gauss–Jordan matrix inversion, as described in Miller (1981), weighting each data point according to its errors.

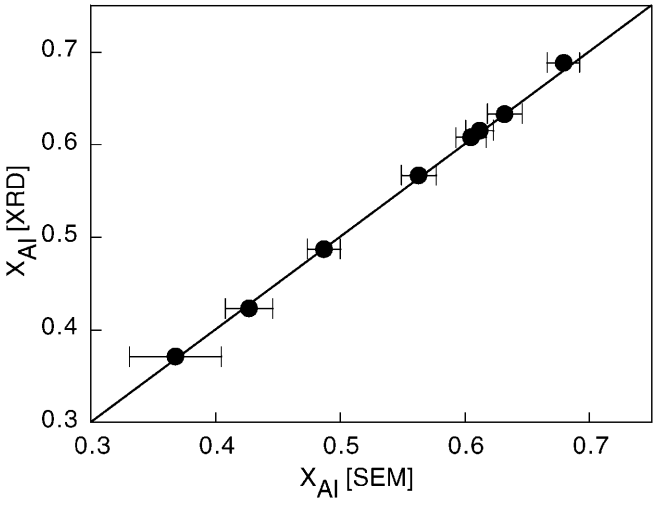

Fig. 1 The Al-content of synthetic titanite (X_{Al}) determined via the unit-cell dimensions with X-ray diffraction (XRD), versus electron microprobe (SEM) data of the same samples. *Solid line* represents ideal correlation. *Error bars* in X_{Al} (SEM) are the standard deviation of the microprobe data

Modelling details

Four types of reaction with Al-rich titanite are considered (non-stoichiometric, and with unspecified additional product and reactant phases):

- Fluid-absent:
  1. Reactants + fluorite = products + $CaAlFSiO_4$
- Fluid-present:
  2. Reactants + hydrous phase + fluorite = products + $CaAlFSiO_4$ + H_2O
- 3. Reactants + carbonate + fluorite = products + $CaAlFSiO_4$ + CO_2
- 4. Reactants + F_2 = products + $CaAlFSiO_4$ + O_2

A binary H_2O–CO_2 fluid is assumed for reactions of types 2 and 3. Ignoring the fluid species HF and F_2 in such equilibria is common practice (e. g. Rice 1980; Barton 1982), as the concentrations of HF and F_2 in metamorphic fluids are extremely low (Munoz and Eugster 1969; Rice 1980; Valley et al. 1982; Droll and Seck 1984; Haselton et al. 1988; Webster and Holloway 1990; Aksyuk and Zhukovskaya 1994). Because HF and F_2, however, do affect the stability of F-bearing phases (e.g. Bohlen and Essene 1978), by analogy to the strong effect oxygen has on many phase equilibria despite its extreme dilution, the effect of F_2 on the stability of AlF-bearing titanite is investigated with reactions of type 4.

The equilibria and titanite X_{Al}-contours were calculated by free energy minimization using the relationships (3) and (4), adopting the MM model for titanite. The equilibria were computed using the calculation methods and data of Berman (1988) for all phases, except for fluorite, $CaAlFSiO_4$, and H_2O below 10 kbar. Fluorite data were taken from Robie and Hemingway (1995), with expansion and compressibility terms from Carmichael (1984) and Birch (1966), respectively. The activity of grossular was calculated with the model of Berman (1990). Fugacities of CO_2, H_2O–CO_2 mixtures and H_2O (below 10 kbar) were calculated with the modified Redlich-Kwong equation proposed by Kerrick and Jacobs (1981). Water fugacities above 10 kbar were computed with the empirical equation of Delany and Helgeson (1978). The fluid pressure equals total pressure.

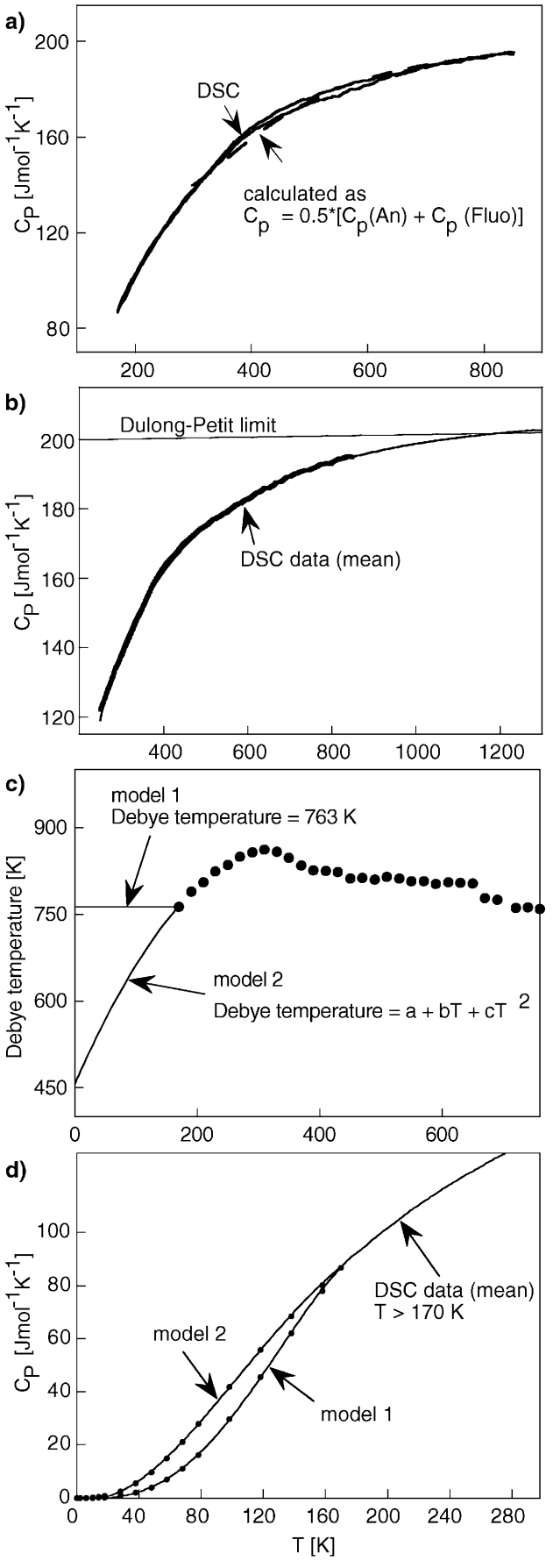

Substitution of F^- for OH^- in hydrous minerals was not considered, and all phases were assumed to be the respective OH end member. Although zoisite in the experiments of Troitzsch and Ellis (1999) contained considerable amounts of fluorine, the assumption that it is F-free in the calculations is justified given that natural zoisite does not seem to incorporate much fluorine even in F-rich rocks (Makanjuola and Howie 1972; López Sánchez-Vizcaíno et al. 1997).

Heat capacity of $CaAlFSiO_4$

The experimentally determined specific heat of $CaAlFSiO_4$ increases smoothly with temperature (Fig. 2a). Both scans deviate less than 3% from the sum of the published heat capacities of anorthite and fluorite. The experimental data are reproduced to within 1% (between 170 and 850 K) by

$$C_P\left(\mathrm{Jmol^{-1}K^{-1}}\right) = 689.96 - 0.38647T + 2911300T^{-2} - 8356.1T^{-0.5} + 0.00016179T^2 \quad (6)$$

The thermodynamic interpretation of the piston-cylinder run products requires the extrapolation of the $CaAlFSiO_4$ heat capacity data to the experimental temperatures (1,073 to 1,273 K). Because no melting was observed in the run products, the heat capacity of $CaAlFSiO_4$ was assumed to increase smoothly beyond 850 K to at least 1,273 K, slowly approaching the 'Dulong-Petit limit' (Gopal 1966; Berman and Brown 1985). The latter was calculated with expansion and compressibility data from Table 2. Figure 2b shows the extrapolation of the heat capacity data (250 to 850 K) to 1,300 K, with an extended Maier and Kelley (1932) heat capacity polynomial (Haas and Fisher 1976)

$$C_P\left(\mathrm{Jmol^{-1}K^{-1}}\right) = 272.54 - 0.01319T - 2055700T^{-2} - 1854.4T^{-0.5} \quad (7)$$

Two dummy points on the DPL at 1,500 K and 1,800 K were included in the fitting procedure, to ensure that the heat capacity smoothly approaches the theoretical limit. A satisfactory fit to the experimental data

◀

Fig. 2 **a** Heat capacity C_P of synthetic $CaAlFSiO_4$ determined with differential scanning calorimetry in two scans (*solid lines*), and estimated from the heat capacities of anorthite (*An*) and fluorite (*Fluo*) (*dashed line*). **b** Extrapolation of experimental heat capacity (DSC data) to 1,300 K with Eq. (9) in the text. The calculation of the Dulong-Petit limit is described in the text. **c** Variation of the Debye temperature of $CaAlFSiO_4$ with temperature. Debye temperatures calculated from calorimetric data above 170 K (*dots*) were extrapolated to absolute zero with two methods (*solid lines*) discussed in the text. Polynomial coefficients of model 2: $a = 456.25$, $b = 2.4175$, $c = -3.5535 \times 10^{-3}$. **d** Low-temperature heat capacity of $CaAlFSiO_4$ (*dots*, T < 170 K) calculated with the extrapolated Debye temperatures of **c**, and experimental heat capacity (*solid line*, T > 170 K). Polynomial functions $y = a + bT + cT^2 + dT^3 + eT^4$ were fitted to the data points between 0 and 170 K (*solid lines*). Model 1 $a = 0.17015$, $b = -0.02873$, $c = 0.00042236$, $d = 4.18116 \times 10^{-5}$, $e = -1.8851 \times 10^{-7}$; model 2 $a = 0.5119$, $b = -0.1602$, $c = 0.0092202$, $d = -3.7612 \times 10^{-5}$, $e = 3.7772 \times 10^{-8}$

Table 2 Thermodynamic properties of $CaAlFSiO_4$, determined with Piston-cylinder experiments (Exp.), X-ray diffraction (XRD) and differential scanning calorimetry (DSC). Lower part of the table shows values used in the data regression, upper part shows results. The calculation of the Gibbs energy of formation was based on the data for the elements of Robie and Hemingway (1995). The regression resulted in $\chi^2 = 0.67$ and $\chi^2 = 1.10$ for the MM and LCB-model, respectively

Property					Method
MM model					
Gibbs energy	d_fG^0	–2,592.9	±1.8	kJ mol^{-1}	
Enthalpy	d_fH^0	–2,740.8	±3.0	kJ mol^{-1}	Exp.
Entropy	S^0	104.9	±1.1	J mol^{-1} K^{-1}	Exp.
Margules parameter	W_H–TW_S	13.6	±0.5	J mol^{-1}	Exp.
LCB model					
Gibbs energy	d_fG^0	–2,587.8	±1.8	kJ mol^{-1}	
Enthalpy	d_fH^0	–2,733.8	±3.1	kJ mol^{-1}	Exp.
Entropy	S^0	111.3	±1.2	J mol^{-1} K^{-1}	Exp.
Margules parameter	W_H–TW_S	–9.1	±0.4	J mol^{-1}	Exp.
Margules parameter	W_V	214	±18	kJ bar^{-1}	XRD
Molar volume	V[a]	5.183		J mol^{-1} bar^{-1}	XRD
Compressibility	v_1	-9.29×10^{-7}		bar^{-1}	[b]
	v_2	2.754×10^{-12}		bar^{-2}	[b]
Expansion	v_3	1.820×10^{-5}		K^{-1}	[b]
	v_4	0		K^{-2}	[b]
Heat capacity	C_P				
	a	272.54		J mol^{-1}	DSC
	b	–0.01319		J mol^{-1} K^{-1}	DSC
	c	–2,055,700		J mol^{-1} K^{2}	DSC
	d	–1,854.4		J mol^{-1} K$^{0.5}$	DSC

[a]Troitzsch et al. (1999)
[b]Assumed to be equal to respective values for titanite: v_1 and v_2 based on Angel (1999); v_3 and v_4 based on Ghose et al. (1991) and Taylor and Brown (1976)

was obtained by allowing the curve to slightly exceed the DPL at higher temperatures (Fig. 2b).

Calorimetric entropy of $CaAlFSiO_4$

The calorimetric entropy of a phase at standard state (1 bar, 298.15 K) can be calculated if its heat capacity is known between 0 K and 298.15 K. Because $CaAlFSiO_4$ heat capacity data are limited to above 170 K, they were extrapolated to 0 K with first principle calculations based on vibrational theory, using the Debye model (e.g. Gopal 1966). Two alternative extrapolations of the Debye temperature to 0 K were considered, in order to cover the entire possible range for entropy values. Model 1 assumes the Debye temperature of 763 K, calculated for the lowest temperature data point, remains constant between 0 and 170 K. Model 2 extrapolates the drop-off in the Debye temperature with a 2nd degree polynomial function fitted to DSC data between 170 and 300 K (Fig. 2c). Figure 2d shows the low temperature heat capacities calculated with these two models. Polynomial functions fitted to the 16 data points of each model yielded the entropy contribution S_{170} from the temperature range 0 to 170 K (Table 3). This was then added to the entropy contribution from 170 to 298 K, obtained from Eq. (6). Because of the sensitivity of the entropy to small errors in the heat capacity at low temperatures, these calculated values should be treated as best possible maximum/minimum estimates for the calorimetric entropy of $CaAlFSiO_4$. Assuming there is neither a low temperature heat capacity anomaly (e.g. caused by a phase transition) nor a configurational contribution to the entropy, the calorimetric entropy (Table 3) can be taken as a first estimate for the standard state entropy of $CaAlFSiO_4$.

An alternative way to estimate the standard state entropy of an unknown substance is to sum the entropies of its components, taking into account any volume or co-ordination differences between the phase and its

Table 3 Estimates of calorimetric entropy of $CaAlFSiO_4$ based on DSC measurements (models 1 and 2, see text and Fig. 2), and on entropies of the components. Entropy values from high P–T experiments are shown for comparison

Method	$S_{170} = \int_0^{170} \frac{C_p}{T} dT$ Debye model (J mol^{-1} K^{-1})	$S_{298} - S_{170} = \int_{170}^{298} \frac{C_p}{T} dT$ Calorimetry (J mol^{-1} K^{-1})	$S^0_{298} = \int_0^{298} \frac{C_p}{T} dT$ (J mol^{-1} K^{-1})
Debye (model 1)	41.5	63.2	104.7
Debye (model 2)	54.9	63.2	118.1
Sum of components	Fyfe et al. (1958)		112.9
	Holland (1989)		120.1
High P–T experiments	MM model		104.9
	LCB model		111.3

constituents. Choosing anorthite and fluorite as components (data from Robie and Hemingway 1995), and based on the method by Fyfe et al. (1958) with volume correction, the entropy of $CaAlFSiO_4$ results in 112.9 ± 0.3 J mol^{-1} K^{-1}. This value lies within the entropy range estimated from combined DSC and first principle calculations (Table 3). The method by Holland (1989), which besides volume changes, accounts for coordination differences between Al in anorthite and $CaAlFSiO_4$, results in a value of 120.1 J mol^{-1} K^{-1}, similar to our Debye extrapolation model 2.

Transition temperature

The the $P2_1/a$ to $A2/a$ phase transition in pure titanite takes place at about 496 K, as indicated by Raman spectroscopy (Salje et al. 1993), TEM (Van Heurck et al. 1991), XRD (Ghose et al. 1991; Chrosch et al. 1997), and infrared spectroscopy (Meyer et al. 1998). Calorimetric studies by Zhang et al. (1995) and Xirouchakis and Tangeman (1998) reported lambda-shaped anomalies at 486 and 483 ± 5 K, respectively, which probably represent the phase transition. Because this phase change takes place in several steps over a certain temperature interval, it is necessary to define which part of the transition is determined here. According to Kek et al. (1997), the onset of the phase transition in pure titanite at 496 K is characterized by the displacement of the Ti atom. This induces anti-phase domain formation, and thus the loss of long-range order within each octahedral chain that characterizes the low temperature phase α with space group $P2_1/a$. Between 496 and 825 K the intermediate phase β is stable (Ca atom on split-position). Titanite with true $A2/a$ symmetry, phase γ, exists above 825 K (Ca atom oscillates between two positions). The most energetic part of this stepwise phase change is its onset at 496 K, which is, therefore, determined in this study. For the sake of consistency with most previous studies, this onset will be termed the $P2_1/a$ to $A2/a$ 'phase transition', or 'phase change', bearing in mind that it probably does not strictly represent the entire $P2_1/a$ to $A2/a$ transformation.

The transition temperature should drop with increasing AlF-content in titanite, reaching room-temperature somewhere between 9 and 18.2 mol% of $CaAlFSiO_4$, as indicated by TEM investigations of previous studies (Troitzsch et al. 1999, and references therein). Measuring the transition temperature of a sample with $X_{Al} = 0.09$ with DSC tested the detection limit of the calorimeter because the transition enthalpy of the titanite phase change is very small (~80 J mol^{-1}, Thiéblot et al. 1999). Moreover, the well-defined lambda-shaped anomaly in the heat capacity of pure titanite (Zhang et al. 1995) can be expected to broaden and 'smear out' with increasing 'impurities' (Meyer et al. 1998) such as Al.

The first heating ramp produced a signal at about 390 K, consistent with a drop in transition temperature as Al increases (Fig. 3a). However, this signal was not

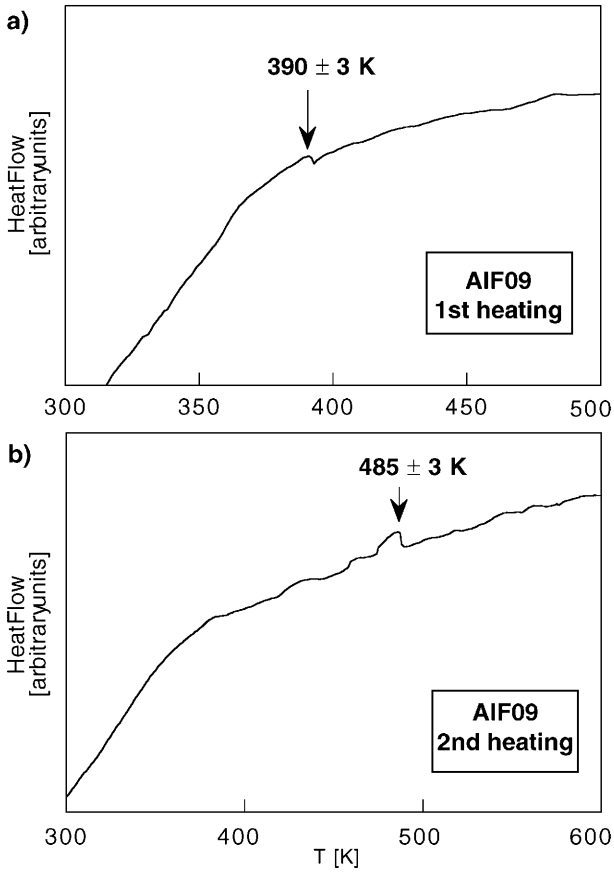

Fig. 3 Heat flow measurement (not converted to absolute heat capacity data; units therefore arbitrary) of sample AlF09. In the light of other methods discussed in the text, the signal detected with the first scan **a** is interpreted to represent the $P2_1/a$ to $A2/a$ phase transition of titanite with $X_{Al} = 0.09$. The signal in the second scan **b** is identical to that of pure titanite, possibly suggesting unmixing of the sample into Al-free and Al-enriched domains

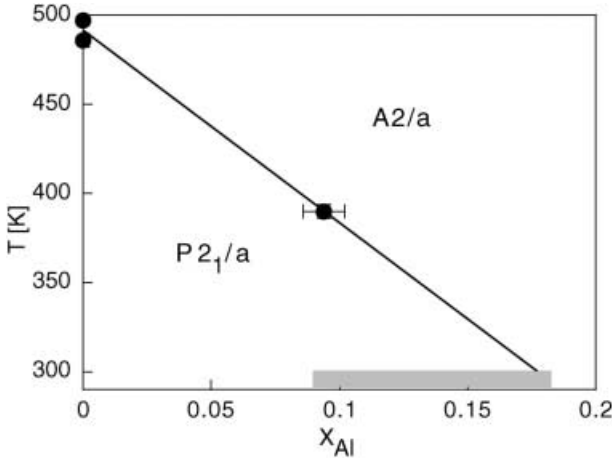

Fig. 4 Section of the phase diagram $CaTiOSiO_4$–$CaAlFSiO_4$, which covers the T–X_{Al} range of the $P2_1/a$ to $A2/a$ phase transition, based on thermal anomalies detected in pure titanite (Salje et al. 1993; Zhang et al. 1995) and sample AlF09 (this study). *Shaded area* represents X_{Al} range of the phase transition at room temperature, based on TEM studies

detected during the second heating of the same sample, where a different signal at 485 K showed instead (Fig. 3b), i.e. the transition temperature observed in end member titanite (Xirouchakis and Tangeman 1998). This may indicate that the Al-bearing sample is exsolving domains of pure titanite composition during multiple heating and cooling. We do not know at this point whether the inferred Al-rich domains in the sample crystallise with the titanite structure or as a different phase.

Figure 4 shows the titanite phase diagram at low Al contents, based on the transition temperature of pure titanite (Salje et al. 1993; Zhang et al. 1995) and sample AlF09. Linear extrapolation of the phase boundary to room temperature predicts the phase change to occur at $X_{Al}=0.179$, consistent with the range of $X_{Al}=0.09$ and 0.182 indicated by previous TEM investigations (Troitzsch et al. 1999). The extrapolation of the transition temperature to 0 K yields a transition composition of $X_{Al}=0.455$, indicating that the end member $CaAlFSiO_4$ probably lies in the $A2/a$ stability field at all temperatures. This is consistent with the assumption made in the above Debye model calculations, of the absence of any low-temperature heat-capacity anomalies.

High P–T experiments and thermodynamic properties of $CaAlFSiO_4$

All run products were composed of anorthite, fluorite and titanite, with or without trace grossular or F-rich zoisite (Table 1). X_{Al} of titanite increases with pressure, but decreases with temperature (Fig. 5a, b), qualitatively confirming the experiments of Smith (1981). However, although X_{Al} in Smith's (1981) assemblage titanite–corundum–rutile–melt did not increase beyond 0.54, but instead levelled out at that value, X_{Al} of titanite coexisting with anorthite and fluorite in this study ranges from 0.282 to 0.914, and even increases more strongly at high pressure.

The generally smooth increase of X_{Al} with pressure is interrupted by a small irregularity between X_{Al} of 0.49 and 0.61 (Fig. 5a). This could reflect underlying crystal structure processes, such as the atomic rearrangement in titanite at this composition (Troitzsch et al. 1999) with its potential effect on the activity. However, the anomaly is within the range of experimental error, and should be noted, but not over-interpreted. Thus, a significant thermodynamic expression of the crystal structural problems at $X_{Al} > 0.6$ identified by Troitzsch et al. (1999) does not exist in the activity–composition relations. Compare, for example, the anomaly observed in the activity of jadeitic pyroxenes, which can be related to ordering processes and change in space group (Holland 1983).

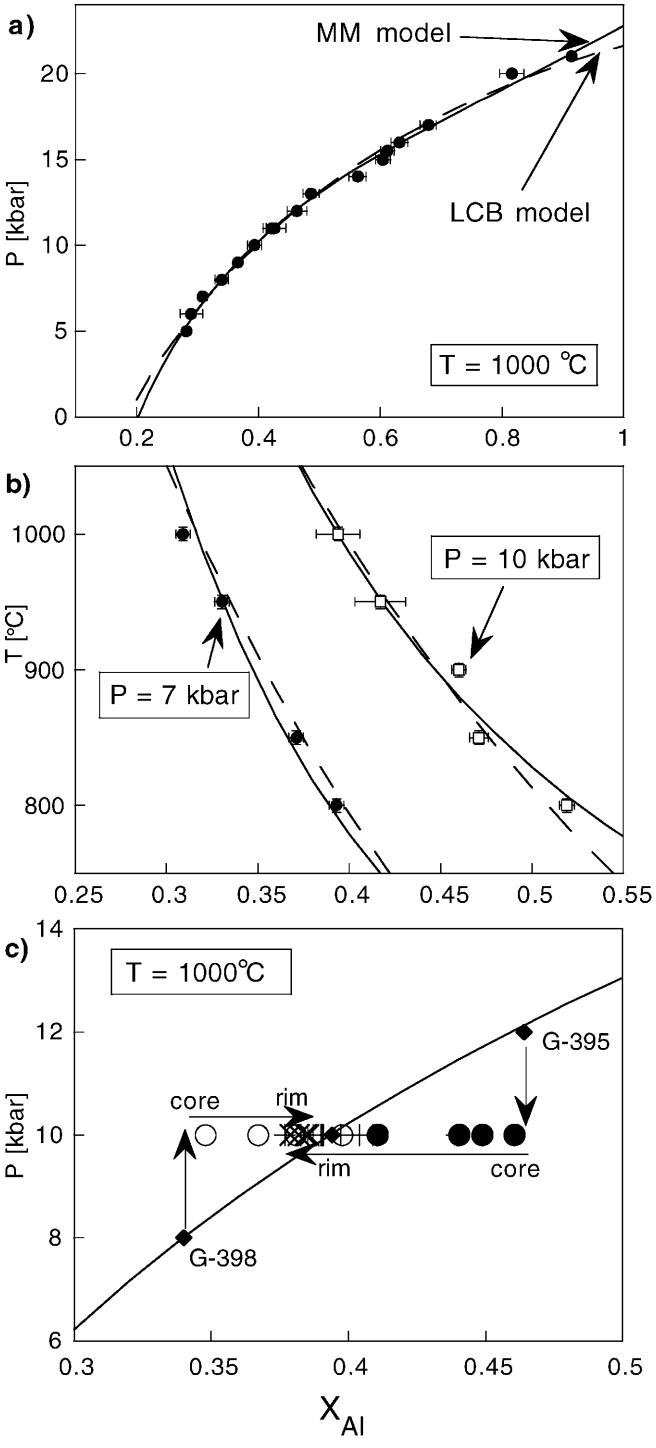

Fig. 5a–c High P–T experimental results. **a** Pressure and **b** temperature dependence of the Al-content (X_{Al}) of titanite coexisting with anorthite and fluorite. *Solid* and *dashed lines* represent the thermodynamic interpretation of the experimental results with a multi-site mixing (*MM*) model and local charge balance (*LCB*) model, respectively (data of Table 2). **c** Titanite composition of two reversal experiments (*large symbols*) compared with previous runs (*small symbols*, and *solid line*). Starting materials of the reversals are characterised by their run number (e.g. G-398, Table 1). *Vertical arrows* indicate pressure difference between previous and reversed runs. *Horizontal arrows* indicate changes in composition from core (*circles*) to rim (*crosses*) of titanite grains in the reversal runs. Reversal of G-395 is shown as *solid circles* and *upright crosses*, G-398 as *open circles* and *diagonal crosses*

All run products of the reversal experiments consisted of anorthite, fluorite and titanite. The titanites were zoned, with cores comparable to the titanite composition of the previously equilibrated run, and the rims approaching the Al content as determined by the main runs at each pressure (Fig. 5c). These 'intermediate' Al contents were approached from both sides, suggesting that the main runs represent near-equilibrium conditions. Because of the compositional zoning of titanites, the reversal experiments were not used in the data regression.

The thermodynamic data of $CaAlFSiO_4$ and the Margules parameter term (W_H–TW_S) obtained from PTX_{Al}-data regression with Eq. (3) are listed in Table 3 (see the Appendix for results referring to different databases). Solid and dashed lines in Fig. 5a, b represent the MM model [Eq. (4)] and LCB-model [Eq. (5)], re#132;spectively. Neither the refinement of asymmetrical Margules parameters, nor the temperature-dependent parameter W_S, improved the regression result for either model, but instead produced unreasonably large errors.

Both mixing models represent the experimental data well, with a slightly smaller χ^2 and therefore better fit for the MM model. For example, at high pressures the LCB-model fails to match the two most aluminous data points (Fig. 5a). The fact that $\chi^2 > 1$ for the MM model indicates that some of the errors used in the data regression are possibly overestimated. The uncertainty of the temperature readings of ± 5 °C is unlikely to be any smaller. However, if the error of the pressure readings was only half of that assumed here (± 0.2 kbar), then χ^2 would be close to unity for the MM model, and respectively higher for the LCB model. Also, it is likely that those errors of X_{Al} are overestimated, which are represented by the standard deviation of SEM analyses (Table 2). If these errors were, for example, only based on the accuracy of SEM analyses (Al ± 1.1 wt%, Ti ± 1.3 wt%), and applied to the average X_{Al} of each sample ($X_{Al} \pm 0.06$), then χ^2 would approach unity, and be respectively larger for the LCB model. Multi-site mixing requires a more negative standard state enthalpy and smaller entropy of $CaAlFSiO_4$ than does molecular mixing (Table 2).

The standard state entropies derived for both mixing models lie within the entropy range determined by calorimetry (Table 3), suggesting no significant additional entropy contributions (e.g. configurational entropy or low T-phase transition). Figure 6 shows the Al content of titanite in the divariant assemblage anorthite–fluorite–titanite, calculated with the Table 2 data. Open diamonds are recent results of Tropper et al. (1999, 2000), indicating run-conditions at which AlF-bearing titanite was equilibrated with anorthite and fluorite ($\pm$ rutile) in piston-cylinder experiments. The good agreement of their data with the predicted Al contents in Fig. 6 demonstrates reproducibility of our experiments, as well as the reliability of the derived thermodynamic properties presented here.

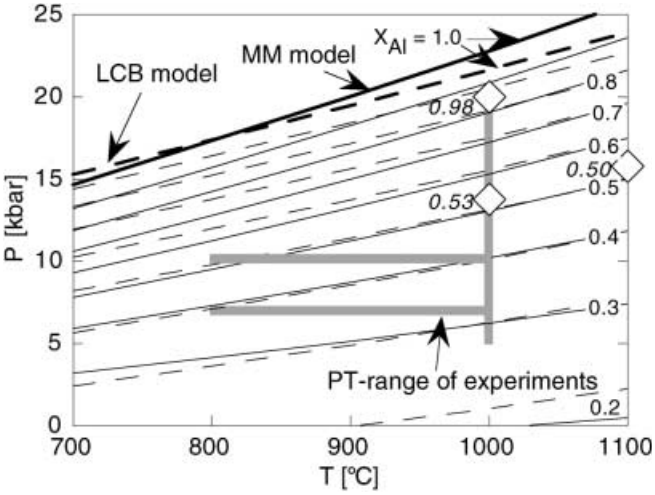

Fig. 6 AlF-content of titanite (X_{Al}) in the divariant assemblage anorthite–fluorite–titanite solid-solution, as predicted by the MM and LCB-model. *Open diamonds* are recent experimental results by Tropper et al. (1999, 2000), indicating run conditions at which titanite was equilibrated with anorthite and fluorite, with or without rutile. The titanite composition they reported is shown in *italics* next to the *symbol*

Mixing model

The Margules parameter (W_H–TW_S) strongly depends on the mixing model (Table 2). While the MM model is consistent with a positive interaction parameter, implying a symmetrical solvus in this binary system, the LCB model requires W_G to be negative, indicating compound formation and thus the absence of a solvus. Although maintenance of local charge balance (LCB model) may seem appropriate for a mixed-charged coupled substitution [reaction (1)], some facts suggest that the MM model represents titanite solid-solution more accurately. First, the MM model yields a slightly better fit to the data than the LCB model (Table 2). Second, when trying to determine the pressure-dependence of the Margules parameter, W_V, from the experimental data, application of the MM model resulted in $W_V = 198 \pm 114$ J mol^{-1} kbar^{-1}, which is in excellent agreement with W_V calculated from the excess volume of mixing based on XRD data (Table 2). In contrast, the LCB model did not permit the determination of W_V at all, but resulted in unreasonably large errors for all refined parameters. The majority of previously reported Margules parameters, determined for other binary solid-solutions, are positive, and only a few cases of negative deviation from ideality are known (Davies and Navrotsky 1981, 1983). Although this should not be used as an argument to dismiss the LCB model as unrealistic, it is nevertheless consistent with our suggestion that the MM model, with positive deviation from ideality, is more appropriate for titanite.

Taylor and Brown (1976) gave a crystal structural explanation as to why the substitution of elements such as Al^{3+} and OH^- (and thus F^-) need not be spatially coupled in titanite. Titanite has chains of TiO_6-octahe-

dra with off-centred Ti-atoms, displaced roughly along the polyhedral chain (e.g. Speer and Gibbs 1976). While in ideal $P2_1/a$-titanite all Ti-atoms within one chain are shifted in the same direction, the commonly observed anti-phase domains are characterized by opposite displacement of Ti compared with the rest of the chain. Three types of O1-site (bridging site between two TiO_6-octahedra) can be distinguished: (1) within an undisturbed octahedral chain with one Ti displaced towards and one away from the O1-site, (2) at a domain boundary with both Ti displaced away from O1, and (3) at a second type of domain boundary with both Ti displaced toward O1. While type-1 sites are relatively charge balanced, type-2 sites are over-saturated with negative charge, and type-3 sites are under-saturated. Taylor and Brown (1976) pointed out that this charge imbalance could be compensated for by the substitution of F^- for O^{2-} in a type-2 site, and the location of Al^{3+} next to a type-3 site, and "emphasised that the substitution of Fe^{3+}, Al^{3+}, and OH^- need not be spatially coupled since the structure at a domain boundary could provide the necessary charge balance". Similarly, Hughes et al. (1997) argued that the coupled substitution of Ca^{2+} and Ti^{4+} by REE^{3+} and Al^{3+} in titanite does not require the occupation of adjacent sites because the charge imbalance caused by an individual substituent could be compensated by anti-phase domain boundaries. Although charge balance along the domain boundaries is plausible for temperatures below the $P2_1/a$–$A2/a$ phase transition (T $<$ 825 K, Kek et al. 1997), where Ti is definitely off-centred and domain formation occurs, its applicability to the high temperatures of the experiments of this study (1,073 to 1,273 K) is uncertain. Also, being based on the Ti position, this concept might not explain the distribution of substituents in Al-dominated titanite.

Potential solvus

If the MM model describes the mixing behaviour of titanite correctly, a solvus exists in the system $CaTiOSiO_4$–$CaAlFSiO_4$. Although non-ideality is generally temperature-dependent, the narrow temperature range of the piston-cylinder experiments did not permit the determination of the Margules parameter W_S. Therefore, solvi calculated with the Margules parameters of Table 2, refer to the experimental temperatures of 800 to 1,000 °C (Fig. 7a). In order to investigate whether a solvus could control the composition of natural lower temperature titanites, W_S has to be estimated. We followed the method described in Pownceby and O'Neill (1994). This estimation is based on the close relation between excess volume and excess entropy (Newton and Wood 1980) by means of its Grüneisen parameter γ. Assuming a Grüneisen parameter similar to that of other solids (compare Poirier 1991, Table 3.3) for $CaAlFSiO_4$ (between 1 and 1.7), and $n = 8$ (atoms per formula unit) yields excess entropies of mixing

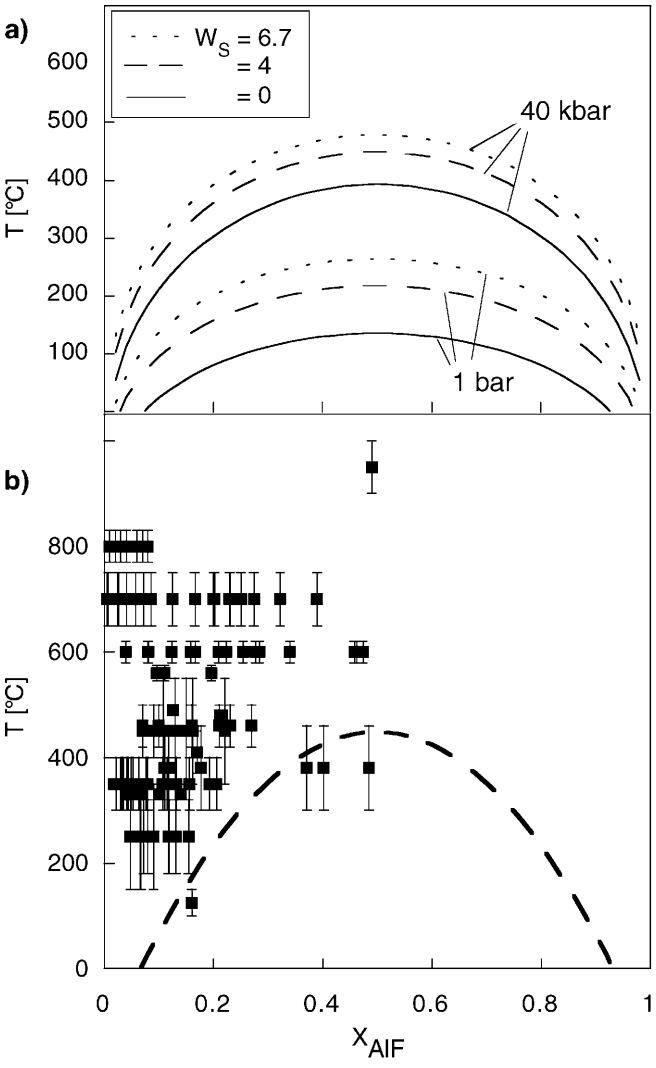

Fig. 7 a Solvi in the binary titanite system as predicted by the MM-model, calculated with different sets of Margules parameters (Table 4), using the equation $T = W_G(2X-1)/(2Rln[X/1-X])$ (Powell 1978). W_S in J mol^{-1} K^{-1}. **b** Al- and F content of natural and synthetic titanites (X_{AlF}, atoms per formula unit of component $CaAlFSiO_4$) versus their temperature of formation (samples refer to various pressures between 0.5 to 40 kbar). The limited composition would be consistent with a solvus (*dashed lines*, placed by eye). *Data points* from (with decreasing temperature): Sobolev and Shatsky (1990), Bernau and Franz (1987), Carswell et al. (1996), Franz and Spear (1985), López Sánchez-Vizcaíno et al. (1997), Enami et al, (1993), Evans and Patrick (1987), Bernau and Franz (1987), Gibert et al. (1990), Yau et al. (1984), Grapes and Watanabe (1992), Makanjuola and Howie (1972), Birch (1983)

Table 4 Different sets of Margules parameters for titanite [Ca(Ti,Al)(O,F)SiO_4], depending on the choice of W_S

W_H[a] (kJ mol^{-1})	W_S (J mol^{-1} K^{-1})	W_V (J mol^{-1} kbar^{-1})
13.6	0.0	214
18.3	4.0	214
21.5	6.7	214

[a]Calculated as $W_H = 13.6 + 1{,}173 W_S$

between 1 and 1.7 J mol^{-1} K^{-1}. The corresponding Margules parameters W_S, calculated with $S^{exc} = W_S X_{Al}(1–X_{Al})$ (e.g. Wood and Fraser 1978) are 4 and 6.7 J mol^{-1} K^{-1}. The Margules parameter term (W_H–TW_S) of 13.6 kJ mol^{-1} refined from the experimental data refers to about 1,173 K (midpoint of the experimental temperature range). For each assumed value of W_S, W_H was calculated with W_H (J mol^{-1}) = 13.6 + 1,173W_S. The resulting sets of Margules parameters are given in Table 4, and the resulting solvi in Fig. 7a. While the critical temperatures of the solvi with $W_S = 0$ lie at high P, low T conditions rarely realized on Earth, the temperature-dependent models predict solvi that would mainly affect titanites from the greenshist-, blueshist- and amphibolite-facies (Fig. 7a).

Figure 7b shows a T–X_{Al} plot of the binary $CaTiOSiO_4$–$CaAlFSiO_4$ system, based on natural titanite analyses that include fluorine, and for which estimates of the equilibration temperatures of titanite were given. Although the samples refer to different pressures (2 to 40 kbar), the general increase in the maximum X_{Al} with increasing temperature (up to $X_{Al} \approx 0.5$) is consistent with the presence of a solvus in this system, with a critical temperature between 400 and 600 °C. This temperature range is comparable to the calculated solvi in Fig. 7a. Note, however, that unmixing textures that would imply a solvus, such as an intergrowth of Al-rich and Al-poor titanite, have never been reported from natural samples. Thermodynamic modelling below shows that the solvus is probably truncated or replaced by other reactions, which could explain the absence of titanite with $X_{Al} > 0.54$.

Thermodynamic modelling

Previous studies of the thermodynamic stability of titanite were exclusively based on $CaTiOSiO_4$ equilibria. In contrast to this, we investigated the stability of AlF-titanite based on the $CaAlFSiO_4$ end member, thus exploring parts of compositional space previously unavailable for titanite.

Because the rare occurrence of natural titanite with $X_{Al} > 0.5$ is yet to be fully understood (Oberti et al. 1991; Troitzsch et al. 1999), the following investigation of phase equilibria in the system CaO–CaF_2–Al_2O_3–SiO_2 ± TiO_2 ± H_2O ± CO_2 focuses on the maximum possible extent of solid-solution in titanite Ca(Ti, Al)(O,F)SiO_4 in various assemblages. Note that the purpose of this paper is not to present P–T grids readily useable for a large range of natural assemblages because there is limited knowledge of fluorine fugacity in natural rocks. Instead, this work will explore and discuss the basic constraints on Al–F in titanite by choosing simple, F-buffered systems, as a first step towards understanding the more complicated ones, such as found in natural rocks. The stability of $CaAlFSiO_4$ was modelled for a hypothetical rock (e.g. F-rich calc-silicate), which should represent an ideal medium for the crystallisation of AlF-rich titanite because it is composed of fluorite, aluminosilicate, quartz and at least one Ca-phase (anorthite, grossular, lawsonite, zoisite, margarite, calcite, depending on fluid species and metamorphic grade), besides titanite solid-solution (Fig. 8).

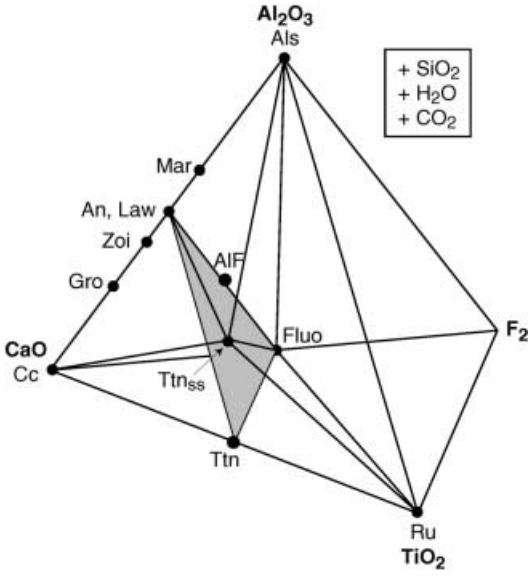

Fig. 8 Tetrahedral phase diagram CaO–Al_2O_3–TiO_2–F_2, projected from SiO_2, H_2O, and CO_2. *Grey plane* represents the ternary system of the experiments of Troitzsch and Ellis (1999). *Stability lines* are shown for assemblages containing titanite solid solution and fluorite. *Abbreviations* in this and following figures: *AlF* $CaAlFSiO_4$, *Als* aluminosilicate, *An* anorthite, *Cc* calcite, *Fa* fayalite, *Fluo* fluorite, *Gro* grossular, *Ky* kyanite, *Law* lawsonite, *M* magnetite, *Mar* margarite, *Q* quartz, *Ru* rutile, *Ttn* titanite, Ttn_{ss} titanite solid solution, *Zoi* zoisite, *V* vapour

Note that this investigation focuses on the binary join TiO–AlF, so that the values of X_{Al} are the amount of aluminium that is substituted with fluorine ($Ti^{4+} + O^{2-} = Al^{3+} + F^-$). In the hydrous model assemblages considered below, titanite would also contain some water (Hammer et al. 1996), so that the total Al content would be the sum of aluminium coupled with fluorine and water. Ignoring the Al–OH end member here is justified given that the most Al-rich natural titanites, which are to be modelled primarily, only contain up to 10 mol% $CaAlOHSiO_4$ (e.g. Franz 1987).

Fluid-absent equilibria

Figure 9a shows the variation of the Al content of titanite in the fluid-absent system CaO–CaF_2–Al_2O_3–SiO_2, which is well constrained in our experiments. The stability fields of grossular and anorthite are given by

$$\underset{\text{Grossular}}{Ca_3Al_2Si_3O_{12}} + \underset{\text{Kyanite}}{2Al_2SiO_5} + \underset{\text{Quartz}}{SiO_2} = 3\,\underset{\text{Anorthite}}{CaAl_2Si_2O_8} \quad (8)$$

The X_{Al}-isopleths of titanite coexisting with fluorite and either anorthite, or grossular, kyanite and quartz,

were determined with Eqs. (3) and (4), for the equilibria (2) and

$$\begin{aligned} 6CaAlFSiO_4 &= Ca_3Al_2Si_3O_{12} + 2Al_2SiO_5 + SiO_2 + 3CaF_2 \\ CaAlFSiO_4 &= \text{grossular} + \text{kyanite} + \text{quartz} + \text{fluorite} \end{aligned} \quad (9)$$

Figure 9a predicts that very Al-rich titanite, including the $CaAlFSiO_4$ end member, should be stable at eclogite facies conditions. The reason why $CaAlFSiO_4$ has not been reported from natural rocks might be that the complete absence of any fluid is an unrealistic assumption, and that anorthite and grossular usually exist in solid-solution. Reduced anorthite and grossular activities would lower the Al content of titanite at a given pressure and temperature. For example, eclogite facies garnets typically contain less than one-third grossular (Deer et al. 1992). The effect of the garnet composition on Al in titanite in this assemblage is shown in Fig. 9b, which was constructed using the garnet composition from titanite-bearing eclogites of the Tauern Window (32 mol% grossular, 57 mol% almandine, 6 mol% pyrope; Franz and Spear 1985). Thus the dilution of the grossular component to values representative of natural mafic rocks restricts the Al content of titanite to less than about $X_{Al} = 0.7$ for typical pressures of crustal metamorphism. Large parts of the stability field of titanite with $X_{Al} > 0.7$ lie beyond the 5 °C km^{-1} geotherm, which approximates the limit of pressure and temperature conditions realised on Earth (Schreyer 1988). The pure $CaAlFSiO_4$ end member would only be stable above 55 kbar, well within the 'forbidden zone', which is in agreement with its absence from natural assemblages.

The wide spacing of the isopleths with respect to pressure in the garnet stability field (Fig. 9) is because of the small ΔV (0.105 J bar^{-1} K^{-1}) of reaction (9). This is so small that it changes from positive to negative at about 250 °C, primarily because of the large thermal expansion of fluorite compared with the other product and reactant phases. The sign change of ΔV leads to a non-singularity of the isotherms because above this temperature the $CaAlFSiO_4$ component will be favoured by high pressures whereas, below 250 °C, it will be favoured by low pressures. This non-singularity is the reason for the change in curvature of the isopleths with decreasing temperature (Fig. 9b). If the ΔV was assumed constant, and equal to that at standard conditions, the slope of the isopleths in Fig. 9b would be negative, and thus qualitatively incorrect, illustrating the importance of expansion and compressibility in thermodynamic calculations such as these.

Fluid-present equilibria: H_2O

Figure 10a shows a simplified version of the CASH system (e.g. Boettcher 1970; Perkins et al. 1980; Chat-

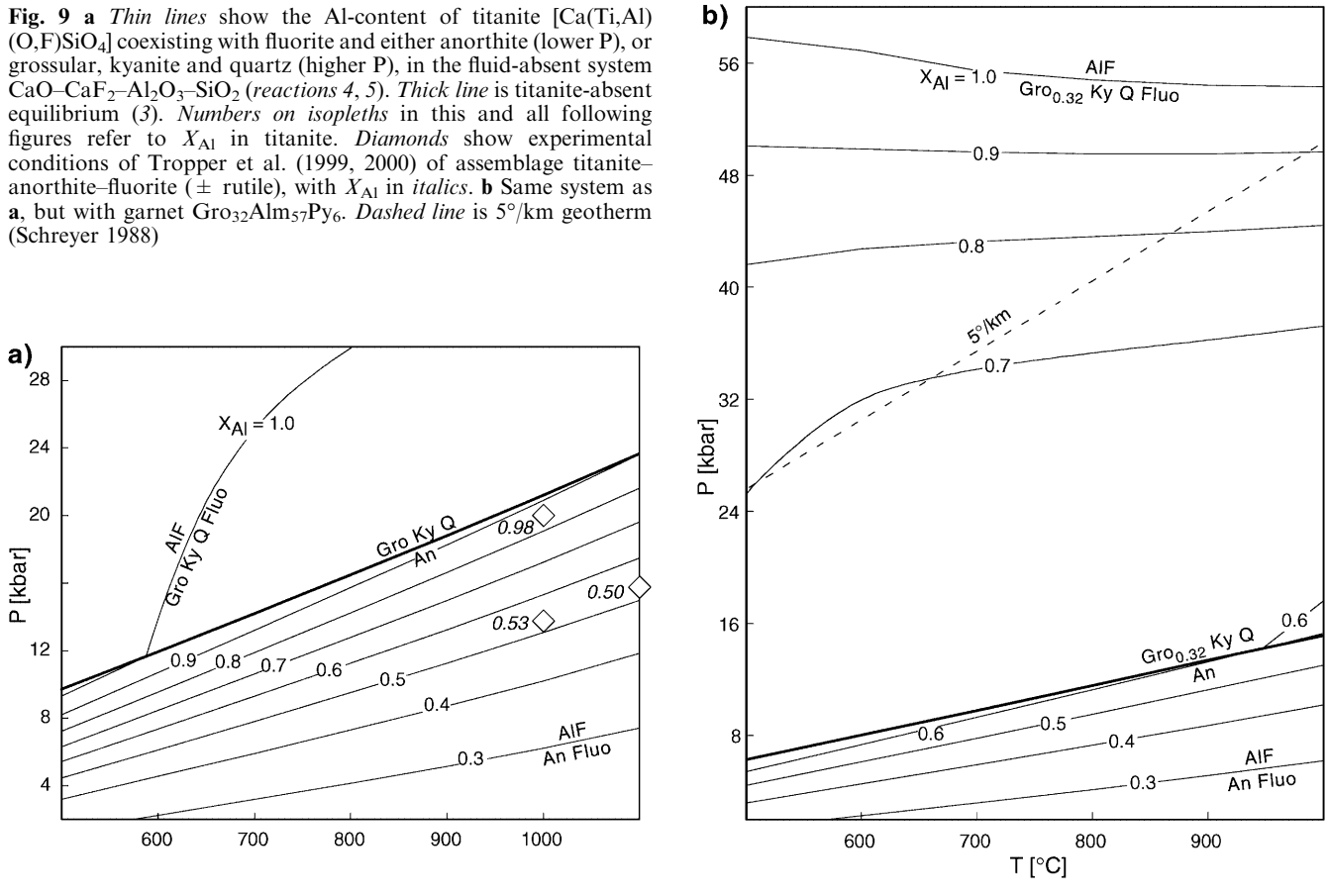

Fig. 9 **a** *Thin lines* show the Al-content of titanite [Ca(Ti,Al)(O,F)SiO_4] coexisting with fluorite and either anorthite (lower P), or grossular, kyanite and quartz (higher P), in the fluid-absent system CaO–CaF_2–Al_2O_3–SiO_2 (*reactions 4*, *5*). *Thick line* is titanite-absent equilibrium (*3*). *Numbers on isopleths* in this and all following figures refer to X_{Al} in titanite. *Diamonds* show experimental conditions of Tropper et al. (1999, 2000) of assemblage titanite–anorthite–fluorite (± rutile), with X_{Al} in *italics*. **b** Same system as **a**, but with garnet $Gro_{32}Alm_{57}Py_6$. *Dashed line* is 5°/km geotherm (Schreyer 1988)

terjee et al. 1984), with contours of the AlF content of titanite coexisting with fluorite and the various CASH phase assemblages. Several other reactions describing the breakdown of margarite with increasing pressure run subparallel to that shown in Fig. 3a (Chatterjee et al. 1984). These reactions are ignored for the sake of clarity and simplicity. For a similar reason, the breakdown of margarite and quartz to anorthite, kyanite and vapour with increasing temperature (Chatterjee et al. 1984) was omitted. All of these reactions produce relatively small divariant fields, with an insignificant effect on the Al content in titanite. The X_{Al}-isopleths are based on reaction (2) and reactions

$$\begin{array}{l} 10CaAlFSiO_4 + 2H_2O = CaAl_4Si_2O_{10}(OH)_2 + 5CaF_2 + 2Ca_2Al_3Si_3O_{12}(OH) + 2SiO_2 \\ CaAlFSiO_4 + H_2O = \text{margarite} + \text{fluorite} + \text{zoisite} + \text{quartz} \end{array} \quad (10)$$

$$\begin{array}{l} 2CaAlFSiO_4 + 2H_2O = CaAl_2Si_2O_7(OH)_2H_2O + CaF_2 \\ CaAlFSiO_4 + H_2O = \text{lawsonite} + \text{fluorite} \end{array}$$

$$\begin{array}{l} 8CaAlFSiO_4 + H_2O = 2Ca_2Al_3Si_3O_{12}(OH) + 4CaF_2 + Al_2SiO_5 + SiO_2 \\ CaAlFSiO_4 + H_2O = \text{zoisite} + \text{fluorite} + \text{kyanite} + \text{quartz} \end{array} \quad (12)$$

The addition of CaF_2 to the CASH system probably lowers the solidus in Fig. 10 by at least several tens of degrees, as suggested by the eutectic melting temperature of the system CaF_2–$Ca(OH)_2$ of 670 ± 10 °C at 1 kbar (Gittins and Tuttle 1964). Two TX-diagrams, derived from Fig. 10a, illustrate the limited extent of solid-solution in titanite at various pressures (Fig. 10b, c).

Because of the topology of the P–T grid in Fig. 10a, the maximum X_{Al} of titanite in this water-saturated system is predominantly controlled by the position of the isopleths in the zoisite stability field. The location of these widely spaced isopleths in P–T space, however, is extremely sensitive to variations in the thermodynamic data used. Errors in the data of any phase in reaction (12) may affect the computed Al content in titanite. For example, by varying the thermodynamic data for $CaAlFSiO_4$ within given errors (e.g. 2 kJ and 1 J 'assumed error' in enthalpy and entropy, respectively), it is possible to create a scenario by which titanite with $X_{Al} > 0.55$ is stable only above 24 kbar and 650 °C, which could potentially explain its absence in nature.

The applicability of Fig. 10a to natural rocks can be significantly improved by considering solid-solution in the Ca–Al phases. Allowing for solid-solution in garnet expands its stability field to lower metamorphic conditions with the reactions (Fig. 10d).

$$\begin{array}{l} 6Ca_2Al_3Si_3O_{12}(OH) = 4Ca_3Al_2Si_3O_{12} + 5Al_2SiO_5 + SiO_2 + H_2O \\ \text{Zoisite} = \text{grossular} + \text{kyanite} + \text{quartz} + H_2O \end{array} \quad (13)$$

$$\begin{array}{l} 4CaAl_2Si_2O_7(OH)_2H_2O = Ca_3Al_2Si_3O_{12} + 2Al_2SiO_5 + SiO_2 + 6H_2O \\ \text{Lawsonite} = \text{grossular} + \text{kyanite} + \text{quartz} + H_2O \end{array} \quad (14)$$

In the stability fields of lawsonite, anorthite, as well as margarite plus zoisite, X_{Al} increases towards the zoisite-only stability field (Fig. 10a). The isopleths in the zoisite stability fields are very widely spaced, so that the increase of X_{Al} with increasing pressure is less in the zoisite than in the anorthite assemblage. Also, the increase of X_{Al} with increasing temperature in the lawsonite field is slowed down in the zoisite assemblage, and is even reversed at higher pressures (Fig. 10b). Thus the occurrence of very Al-rich titanite is restricted to high metamorphic grades. Titanite with $X_{Al} > 0.6$ predominantly occurs at eclogite facies conditions, and Al-contents of $X_{Al} > 0.8$ are restricted to a small wedge-shaped P–T window at very high grade, which might even be limited by melting reactions at higher pressures before the stability of the $CaAlFSiO_4$ end member is reached.

In contrast to grossular, zoisite and lawsonite form less extensive solid-solution. Again, the rocks of the Tauern Window (Franz and Spear 1985) were used as a representative example for an eclogite facies rock with titanite. The activities of the phases were calculated according to the study by Manning and Bohlen (1991) ($a_{Zoi} = 0.833$, grossular activity based on Berman 1990). The titanite Al-isopleths in the zoisite stability field move to slightly higher pressures because of the dilution of zoisite. More importantly, the zoisite stability field is cut off by grossular before the $X_{Al} = 0.7$ isopleth is reached (compare Fig. 10a). Because the isopleths in the grossular stability field are even more widely spaced compared with those in the zoisite field (isopleth $X_{Al} = 0.7$ lies outside the P–T range shown here), the stability of titanite with $X_{Al} > 0.7$ is restricted to significantly higher metamorphic grades compared with the end member calculations.

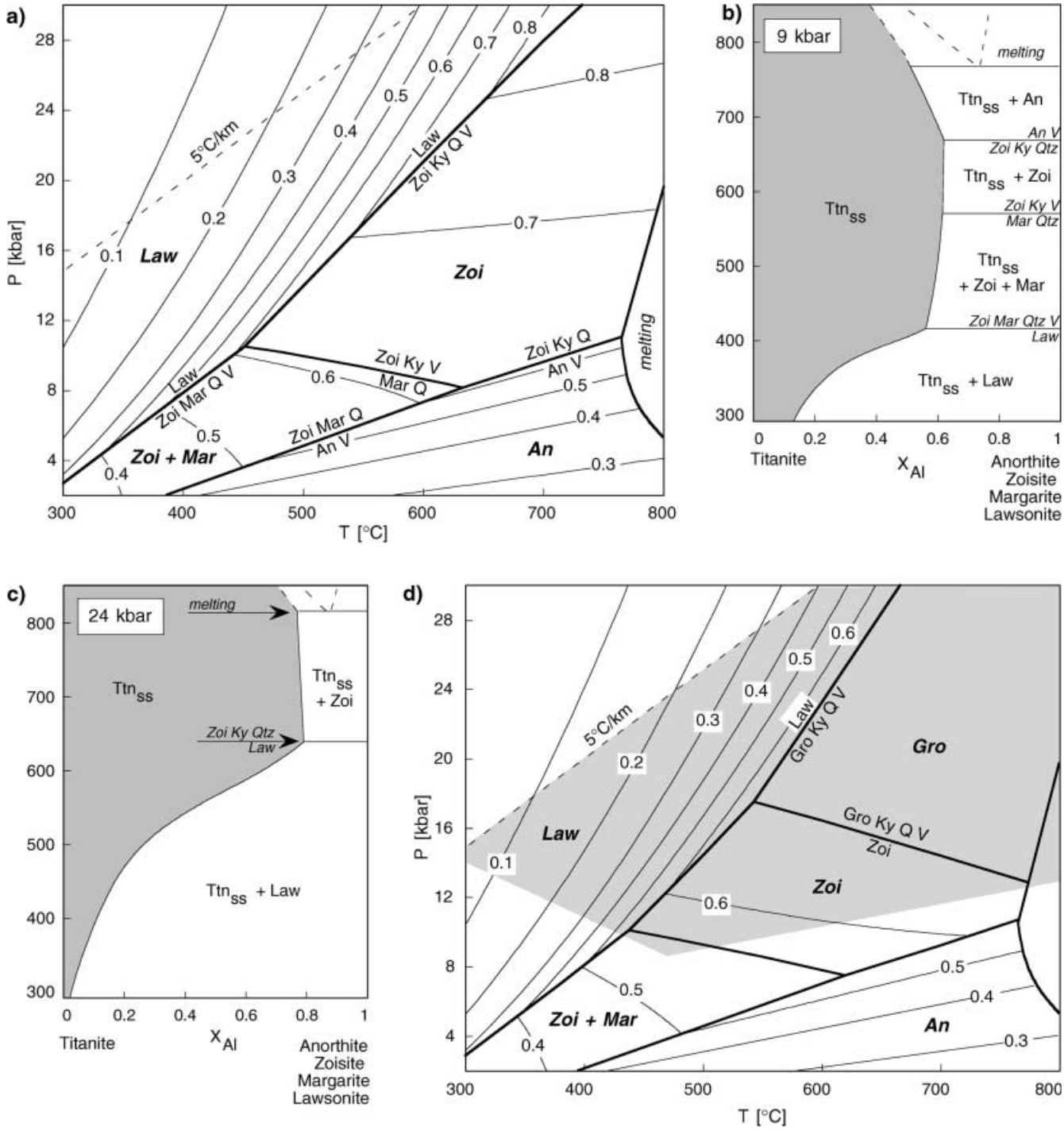

The topology of Fig. 10d is consistent with the natural occurrence of aluminous titanite, in that titanite with $X_{Al} < 0.6$ can be stabilized at pressures and temperatures covering many metamorphic facies, but the most likely occurrence of Al-rich titanite is at eclogite facies conditions. This is consistent with the numerous reports of Al-rich titanite from eclogite terrains (e.g. Smith 1980; Franz and Spear 1985; Krogh et al. 1990; Sobolev and Shatsky 1990; Hirajima et al. 1992; Carswell et al. 1996; Ye and Hirajima 1996), and the less abundant, yet important finds of Al-rich titanite from lower metamorphic grade (e.g. Boles and Coombs 1977; Franz 1987; Enami et al. 1993; Markl and Paizolo 1999). At temperatures below 450 °C, titanite does not incorporate more than $X_{Al} = 0.55$ at any pressure. The blueschist facies is especially dominated by lower Al contents, which is in good agreement with natural titanites from such high-pressure, low-temperature terrains typically containing less than $X_{Al} = 0.20$ (e.g.Makanjuola and Howie 1972; Itaya et al. 1985).

◀

Fig. 10 **a** Al-content of titanite in the fluid-present system CaO–CaF_2–Al_2O_3–SiO_2–H_2O ($P_{H_2O} = P_{total}$). *Bold lines*: reactions of the CASH-system, with the stability fields of the different Ca–Al phases labelled in *bold*. *Thin lines* X_{Al}-isopleths based on *reactions* (*4*) and (*6*) to (*8*) in the stability fields *An*, *Mar* + *Zoi*, *Law*, and *Zoi*, respectively. *Solidus* in this and subsequent figures refers to the pure CASH system (Thompson and Ellis 1994). **b**, **c** Isobaric T–X_{Al} plots ($P_{H_2O} = P_{total}$) of the pseudo-binary system TiO_2–$AlO_{1.5}$, based on **a**, illustrating the limited extent of solid-solution of titanite in various assemblages with fluorite. Phase compositions in the melting region are semi-quantitative estimates. **d** Effect of solid-solution in grossular and zoisite on calculated reactions in the CASH system and titanite X_{Al} isopleths (**a**) ($X_{Gro} = 0.32$, $a_{Zoi} = 0.833$). Eclogite facies *shaded*

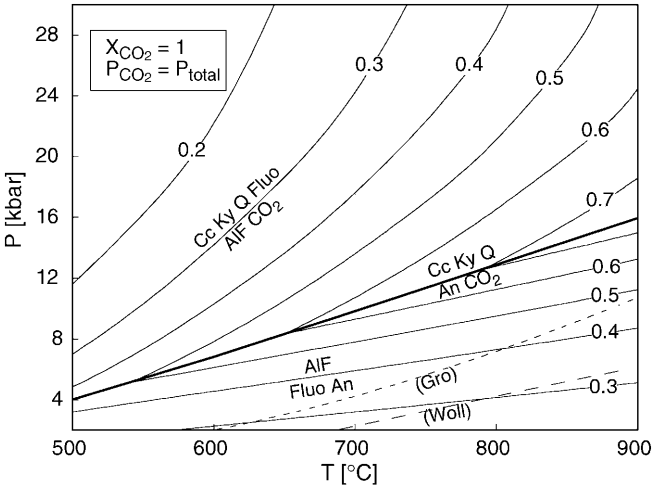

Fig. 11 Al-content of titanite, coexisting with a pure CO_2-fluid in the system CaO–CaF_2–Al_2O_3–SiO_2–CO_2. Grossular is absent, as the reaction calcite + kyanite + quartz = grossular + CO_2 (*Gro*) is metastable. Also shown is reaction calcite + kyanite = wollastonite + CO_2 (*Woll*). Melting at or below 880 ± 10 °C (eutectic temperature in the binary system CaF_2–$CaCO_3$ at 1 kbar, Gittins and Tuttle 1964)

The Al and F contents of titanite in the Tauern Window rocks span a large range, with a maximum value of $X_{AlF} = 0.54$ in one fluorite- and zoisite-bearing rock (sample 79-102, Franz and Spear 1985). The peak metamorphic conditions of these rocks, at which the Al-rich titanite is thought to have equilibrated, are 20 ± 2 kbar, 600 °C, with an almost pure H_2O-fluid (Franz and Spear 1983). At these conditions, however, Fig. 10d predicts Al contents of about $X_{Al} = 0.65$. This inconsistency could be because not all phases of the buffer assemblage are present in this sample (quartz and kyanite were not mentioned by Franz and Spear 1985). More likely, it could simply be because of the large uncertainties attached to the isopleth position, which can be estimated to be of the order of $X_{Al} \pm 0.25$ for the zoisite stability field. This uncertainty is enormous in petrological terms, and rules out the confident use of titanite as a geothermobarometer in this assemblage.

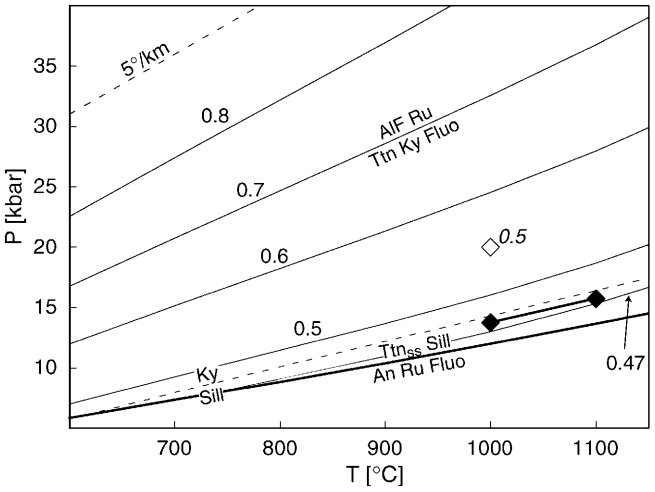

Fig. 12 Al-content in titanite, coexisting with rutile, kyanite and fluorite [reaction (15)]. *Bold line* is reaction (16) referring to $X_{Al} = 0.45 \pm 0.03$. *Open diamond* shows experimental conditions of Tropper et al. (1999) of assemblage titanite–fluorite–kyanite–rutile, with X_{Al} given in *italics*. *Black diamonds* represent stability limit of the assemblage anorthite–rutile–titanite–fluorite in experiments by Tropper et al. (2000; X_{Al} as in Fig. 9a)

Fluid-present equilibria: CO_2

High grade metamorphic fluids such as in granulites are typically CO_2-rich. Figure 11 shows the AlF content of titanite in equilibrium with CAS–CO_2 phases, described by the reactions

$$\begin{aligned} &CaCO_3 + Al_2SiO_5 + SiO_2 = CaAl_2Si_2O_8 + CO_2 \\ &\text{Calcite} + \text{kyanite} + \text{quartz} = \text{anorthite} + CO_2 \end{aligned} \quad (15)$$

$$\begin{aligned} &CaCO_3 + Al_2SiO_5 + SiO_2 + CaF_2 = 2CaAlFSiO_4 + CO_2 \\ &\text{Calcite} + \text{kyanite} + \text{quartz} + \text{fluorite} = CaAlFSiO_4 + CO_2 \end{aligned} \quad (16)$$

Figure 11 demonstrates that $P_{CO_2} = P_{total}$ restricts the Al content of titanite, yet again, to less than about $X_{Al} = 0.75$, at crustal conditions. Although at higher pressure the isopleths of the decarbonation reaction (16) swing back to lower temperatures, titanite with $X_{Al} > 0.7$ becomes stable again only at extremely high pressures (for example, 55 kbar at 750 °C), possibly not realised in natural rocks.

Equilibria with TiO_2

A simple fluid-absent reaction relating the two titanite end members is (Fig. 12)

$$\begin{aligned} &2CaAlFSiO_4 + TiO_2 = CaTiOSiO_4 + Al_2SiO_5 + CaF_2 \\ &CaAlFSiO_4 + \text{rutile} = \text{titanite} + \text{aluminosilicate} + \text{fluorite} \end{aligned} \quad (17)$$

Again, natural titanite with extremely high Al contents and the $CaAlFSiO_4$ end member are not to be expected in this assemblage because their isopleths lie beyond the 5 °C-km^{-1} geotherm. The assemblage titanite–rutile–

aluminosilicate–fluorite [equilibrium (17)] is limited towards lower pressure by the breakdown of titanite ($X_{Al} = 0.45 \pm 0.03$) and sillimanite by the reaction

$$[(1-n)CaTiOSiO_5 + nCaAlFSiO_4] + (1-n)Al_2SiO_5 = (1-n/2)CaAl_2Si_2O_8 + (n/2)CaF_2 + (1-n)TiO_2$$

$$\text{Titanite}_{SS} + \text{Sillimanite} = \text{Anorthite} + \text{Fluorite} + \text{Rutile} \quad (18)$$

where $n = X_{Al}$. This equilibrium is simply the summation of the two reactions limiting the stability of each end member, i.e. reaction (2) and

$$CaTiOSiO_4 + Al_2SiO_5 = CaAl_2Si_2O_8 + TiO_2$$
$$\text{Titanite} + \text{aluminosilicate} = \text{anorthite} + \text{rutile} \quad (19)$$

The displacement of this reaction in the presence of fluorite, which allows for titanite solid-solution along the binary join TiO–AlF discussed here, was investigated recently with piston-cylinder experiments by Tropper et al. (1999, 2000). They reported titanite with $X_{Al} = 0.50$ from the synthetic assemblage titanite–rutile–kyanite–fluorite at 20 kbar and 1,000 °C (open diamond, Fig. 12), which agrees well with the predicted $X_{Al} = 0.55$ isopleth of equilibrium (17). Tropper et al. (2000) determined the stability limit of the assemblage anorthite–rutile–titanite–fluorite (black diamonds, Fig. 12), which differs less than 2 ± 0.2 kbar from that calculated here with reaction (17).

The stability of titanite in calcareous rocks can be described by the reaction

$$CaCO_3 + SiO_2 + TiO_2 = CaTiOSiO_4 + CO_2$$
$$\text{Calcite} + \text{quartz/coesite} + \text{rutile} = \text{titanite} + CO_2 \quad (20)$$

This equilibrium restricts titanite in the presence of a pure CO_2 fluid to low pressures and high temperatures (Fig. 9; Hunt and Kerrick 1977; Jacobs and Kerrick 1981). As pointed out previously (Carswell et al. 1996; Frost et al. 2001) the stability of titanite can be extended to higher pressures by diluting the CO_2 content of the fluid, as well as by diluting the titanite component in solid-solution. This explains the presence of Al-rich titanite in calcareous eclogite-facies rocks, such as the carbonate-bearing eclogites from Dabieshan (Carswell et al. 1996), siliceous dolomites in eclogite facies rocks of the Tauern Window (Franz and Spear 1985), and the calc-silicates and marbles in the eclogite complex at Tromsø (Krogh et al. 1990). This effect is demonstrated in Fig. 13 with the rocks from the Tauern Window, which equilibrated at eclogite-facies conditions in the presence of an almost pure H_2O-fluid (Holland 1979; Franz and Spear 1983, 1985). The dilution of both the titanite component with $CaAlFSiO_4$ (maximum $X_{Al} = 0.54$, Franz and Spear 1985), and the CO_2 fluid with H_2O, shifts the reaction to pressures just high enough to stabilise titanite at the given metamorphic conditions.

Fluorine fugacity

Previous studies showed that the titanite composition depends on the fugacities of oxygen and fluorine (Markl and Piazolo 1999). For example, Bohlen and Essene (1978) investigated fluorine-rich assemblages from several locations in the Adirondacks, USA, and the buffering effect on fluorine and oxygen fugacities. According to their calculations, the stability of titanite is restricted to low fluorine fugacities with the reaction (Fig. 14)

$$2CaTiOSiO_4 + 2F_2 = 2CaF_2 + 2TiO_2 + 2SiO_2 + O_2$$
$$\text{Titanite} + F_2 = \text{fluorite} + \text{rutile} + \text{quartz} + O_2 \quad (21)$$

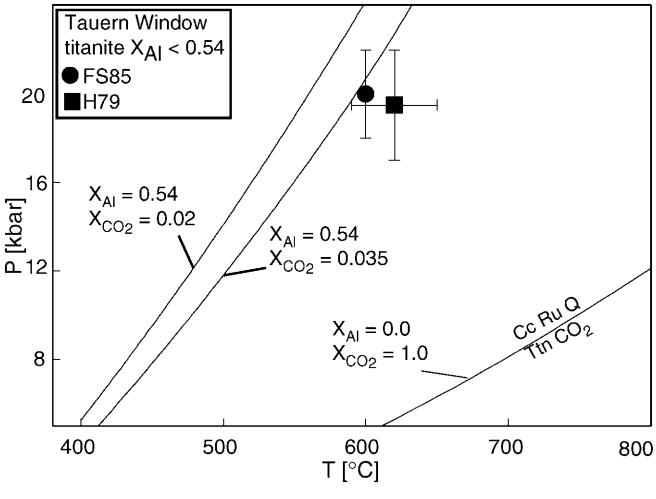

Fig. 13 Dependence of reaction (18) on X_{Al} of titanite and the X_{CO_2} of the coexisting fluid ($P_{fluid} = P_{total}$). *Data points* represent peak-metamorphic conditions for titanite-bearing eclogites from the Tauern Window. Estimates of fluid composition are $X_{CO_2} = 0.02$ (Holland 1979) and $X_{CO_2} = 0.035$ (Franz and Spear 1983). *FS85* Franz and Spear 1985; *H79* Holland 1979. Calcite–aragonite transition not shown

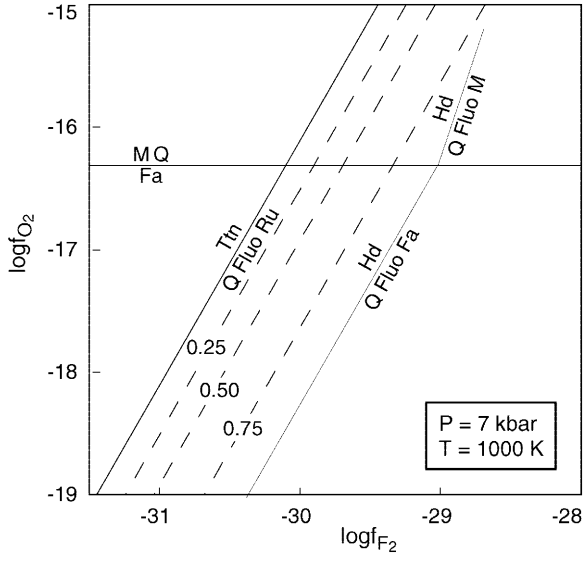

Fig. 14 *Bold lines* are reactions (21) and (22) calculated using thermodynamic data given in Bohlen and Essene (1978). *Dashed lines* are titanite X_{Al}-isopleths

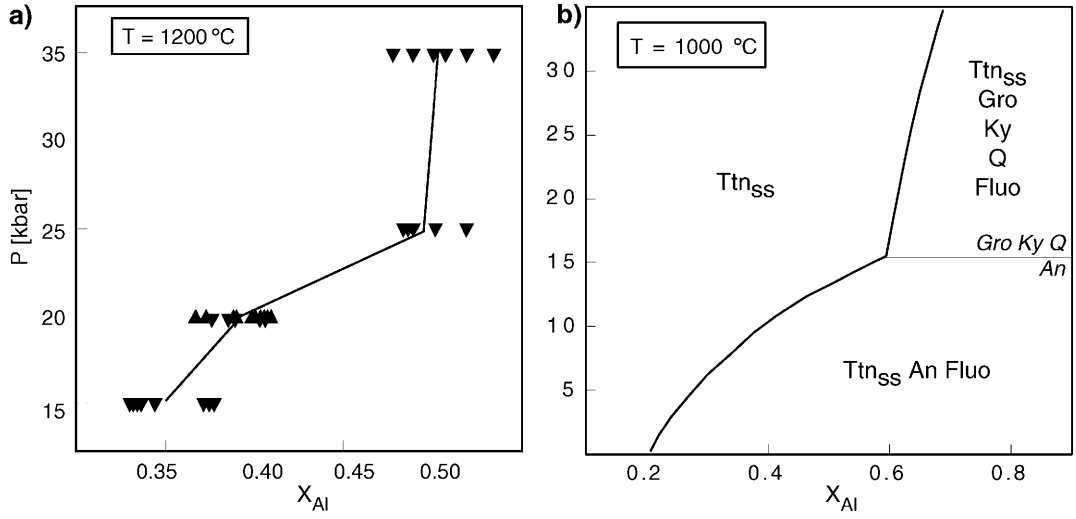

Fig. 15 Pressure dependence of Al in titanite based on **a** experiments by Smith (1981), and **b** thermodynamic modelling in the system of Fig. 9b. See text

whereas the assemblage hedenbergite–quartz–fluorite–fayalite is restricted to higher f_{F_2} with reaction

$$\begin{aligned} &2CaFeSi_2O_6 + 2F_2 = 2CaF_2 + Fe_2SiO_4 + 3SiO_2 + O_2 \\ &\text{Hedenbergite} + F_2 = \text{fluorite} + \text{fayalite} + \text{quartz} + O_2 \end{aligned} \quad (22)$$

In agreement with this, Bohlen and Essene (1978) found the assemblage hedenbergite–quartz–fluorite–fayalite without titanite in the Wanakena fayalite–granite. However, they noted that Leonard and Buddington (1964) reported titanite in the same rock. This would pose a problem if the titanite was in equilibrium with the assemblage described by Bohlen and Essene (1978). They suggested that either uncertainties in the thermodynamic data, particularly those of titanite, could account for this possible inconsistency, or that the titanite contains additional components, which extend its stability field to higher fluorine fugacities. Although analyses of this titanite were not reported, the high fluorine content of the rocks suggests that the titanite may contain Al and F, which could extend its stability field. Figure 14 shows the shift of reaction (22) with increasing $CaAlFSiO_4$ content of titanite. Even Al contents as high as $X_{Al} = 0.75$, which exceeds all values previously reported from natural rocks, cannot extend the stability of titanite sufficiently to overlap with the assemblage hedenbergite–quartz–fluorite–fayalite. Note that reaction (22) is calculated for the end member phases. If phase compositions of the Wanakena granite were considered, this equilibrium would plot at slightly higher fluorine fugacities, thus even further away from the titanite stability field (Bohlen and Essene 1978). Because Al in titanite cannot reconcile the calculations with the observations, it can be concluded that the inconsistency between the calculated petrogenetic grid by Bohlen and Essene (1978) and the observed mineral assemblage, must be caused by errors in the thermodynamic data they used. If the same reactions are calculated with the data from Robie and Hemingway (1995), the titanite stability field overlaps with the hedenbergite–quartz–fluorite–fayalite assemblage, and the problem reported by Bohlen and Essene (1978) is resolved.

Summary and conclusions

The $CaTiOSiO_4$–$CaAlFSiO_4$ activity–composition relations and mixing models provide important information for future thermodynamic studies of titanite as a petrogenetic indicator. The effect of the fluorine fugacity on the Al content of titanite can now be quantified via the end member $CaAlFSiO_4$. Future work on the water-bearing end member ($CaAlOHSiO_4$) is highly desirable in order to extend the application of Al–titanite equilibria to a wider range of natural rocks.

The calculated P–T grids agree with natural occurrences of Al-bearing titanite in many aspects. Titanite solid-solution with up to $X_{Al} = 0.6$ can occur in most metamorphic facies, but more Al-rich titanites are generally restricted to eclogite facies conditions. Titanite with $X_{Al} > 0.8$, and the pure $CaAlFSiO_4$ end member can only be stable at pressures and temperatures accessible to crustal metamorphism in the absence of any fluid, be it H_2O or CO_2, and if the coexisting garnet is pure grossular. These conditions, however, might never be realised in nature. In more realistic scenarios accounting for garnet solid-solution and/or the presence of a fluid, titanite with $X_{Al} > 0.75$ does not occur, either because it is restricted to extremely high pressures rarely realised in natural rocks (Figs. 9b and 11) or because it is unstable with respect to other phases or melt (Fig. 10b). While the presence of H_2O destabilises high concentrations of $CaAlFSiO_4$ with respect to zoisite or grossular (Fig. 10d), a CO_2-bearing fluid promotes its breakdown to an assemblage with calcite (Fig. 11). This confirms the hypothesis of Troitzsch and Ellis (1999) that very Al-rich

titanite and $CaAlFSiO_4$ are only stable in simple chemical systems such as in experiments, and reconciles the apparent contradiction between the synthesis of $CaAlFSiO_4$, and its absence from natural rocks. The calculated P–T grids also suggest that the blueschist facies is dominated by titanite of lower Al content, which is in good agreement with natural observations.

The last point illustrates that the simple relationship between pressure, temperature and titanite composition, as observed in our experiments and those of Smith (1981; i.e. increasing pressure and decreasing temperature promote Al in titanite), cannot be used as a 'rule of thumb', but depends on the buffering effect of the specific mineral assemblage. The Al content of titanite equilibrated with lawsonite and fluorite, for example, behaves inversely because of the large volume contribution of the fluid phase (Fig. 10a).

Reactions such as Eq. (20) seem to be good indicators for pressure–temperature–fluid composition relationships (Fig. 13). In contrast, the extremely widely spaced X_{Al}-isopleths in high-pressure assemblages with zoisite and grossular are very sensitive to changes or errors in the input data. Thus, the uncertainties attached to the Al content computed with these equilibria are very large and do not allow the use of Al in titanite as a reliable geothermobarometer. Such widely spaced isopleths may in fact be responsible for the 'levelling out' of the Al contents in titanite at about $X_{Al} = 0.53$ between 25 and 35 kbar in the experiments by Smith (1981). This is suggested by the striking similarity between the P–X_{Al} plot by Smith (1981), and that, for example, based on Fig. 9b of this study (Fig. 15). According to Smith (1981) various phase assemblages occur in his experiments (titanite–rutile–corundum-melt with either kyanite, quartz or fluorite), thus allowing for a possible reaction between 20 and 25 kbar to explain the change in slope (Fig. 15a). Unfortunately, this system cannot be modelled in detail because the assemblages for individual experiments were not given by Smith (1981). Moreover, the presence of melt prevents straightforward thermodynamic modelling.

The multi-site mixing model of titanite used throughout the present study implies the existence of a solvus in the binary TiO–AlF titanite system. This seems to be contradicted by the lack of reports of natural titanite unmixing into Al-rich and Al-poor domains, but may be explained, for example, with Fig. 10b, c. Here the solvus would lie in the Ttn_{SS} + Law field. Although the curved shape of the Ttn_{SS} + Law stability field at low Al contents suggests that the solvus is approached, it is not reached because very Al-rich titanite is not stable in this wet system. The stability field of Ttn_{SS} (shaded in Fig. 10) is cut off at high Al contents by reactions stabilising other Ca–Al phases and fluorite. Because of the instability of very Al-rich titanite in most systems, the situation in Fig. 10b, c may be typical for Al–titanite in general. Instead of unmixing into two titanite phases, the breakdown of Al-rich titanite to a vermicular intergrowth of Al-poor titanite and anorthite can be observed in rocks (Carswell et al. 1996).

The instability of the $CaAlFSiO_4$ end member with respect to other phases in almost all assemblages investigated here is in very good agreement with the crystal structure data of Troitzsch and Ellis (1999) and Troitzsch et al. (1999), which indicate that the titanite structure is not well suited to accommodate Al and F instead of Ti and O. High bond valence sums at the Ca and O1-site, and polyhedral distortion, indicate structural stresses, lattice energies of small magnitudes, and thus low thermodynamic stability of $CaAlFSiO_4$ (i.e. high Gibbs free energy), manifested in its standard state properties. The limiting value of $X_{Al} = 0.65 \pm 0.15$ observed in the P–T grids presented here supports the hypothesis based on crystal structure data that titanite stability decreases when X_{Al} exceeds 0.6 significantly (Troitzsch et al. 1999). Note, however, that the activity–composition relations are simple, without any significant anomaly at high Al contents, which could be the thermodynamic expression of the crystal structural problems setting in at about $X_{Al} = 0.65$. Thus, the limiting composition of titanite in the petrogenetic grids cannot be linked directly to the crystal structural problems observed at these Al contents via the activity of titanite. There does not seem to be a particular 'catastrophic' crystal structural process, such as the collapse of the octahedral bonds at $X_{Al} = 0.40$ (Troitzsch et al. 1999), which could act as an energy barrier, preventing high Al-titanite formation, as this would show in the activity–composition relations. Rather, it seems to be continuous crystal structural changes that affect the thermodynamic stability of titanite, such as the smooth change in bond valence sums from one end member to the other (Troitzsch et al. 1999), which might not stand out as anomalies in activity–composition relationships.

Thus, the structural problems at $X_{Al} > 0.60$, and the limiting composition in the petrogenetic grids have the same cause, i.e. the incorporation of an increasing amount of an end member with a less suited structure and thus lower thermodynamic stability. The maximum Al content of natural titanites of $X_{Al} \approx 0.54$, is probably simply marking the point beyond which the thermodynamically less favourable $CaAlFSiO_4$ starts to dominate over $CaTiOSiO_4$ in the solid-solution.

Acknowledgements This work was funded by an ARC grant on titanite equilibria to D.J. Ellis, and ANU-PhD and OPRS scholarships to Ulrike Troitzsch. Reviews by Alison R. Pawley and Tim Holland improved the manuscript. DSC experiments were carried out at RSC, ANU.

Appendix

Table A1

Coefficients of curve fit polynomials representing the unit-cell dimensions a, b and c, as used for the indirect

determination of the composition of fine-grained, synthetic titanite. The polynomials are defined as

$$Y_{a,b,c,\beta,V,BVS} = \sum (M_n)_{a,b,c,\beta,V,BVS}\, X^n \quad \text{with n} = 0, 1, \ldots, 5.$$

whereby X represents the independent variable X_{Al}, Y is the dependent variable a, b, or c, and M_n are the polynomial coefficients.

Unit cell dimension	a [Å]	a [Å]	b [Å]	c [Å]
X_{Al} range	0.00–0.18	0.18–1.00	0.00–1.00	0.00–1.00
M_0	7.0612	7.0477	8.7135	6.5583
M_1	–0.4906	0.0675	–0.3005	–0.2159
M_2	9.8272	–0.2876	0.6571	0.6507
M_3	–84.343	0.0886	–1.6357	–1.5301
M_4	322.67		1.727	1.5398
M_5	–460.46		–0.6529	–0.5628

Table A2

Enthalpy of formation from the elements (d_fH^0) and the standard state entropy (S^0) of $CaAlFSiO_4$, and Margules parameter at experimental temperature (W_H–TW_S), determined with various thermodynamic data for anorthite (Anor) and fluorite (Fluo). Data bases: Robie and Hemingway (1995; RH), two updates of the program SUPCRT (Johnson et al. 1991; SUP94 and SUP98), Holland and Powell (1998; HP). The calculation of the Gibbs energy of formation (d_fH^0) was based on the data for the elements by Robie and Hemingway (1995). The standard state is 298.15 K and 1 bar.

Data Anor	Data Fluo	MM-model	LCB-model
		d_fH^0 (kJ mol^{-1})	d_fH^0 (kJ mol^{-1})
RH	RH	–2,743.7 ± 3.0	–2,736.7 ± 3.1
HP	RH	–2,744.3 ± 2.0	–2,737.3 ± 2.1
SUP94	SUP94	–2,741.1 ± 3.0	–2,734.1 ± 3.1
SUP98	SUP98	–2,734.0 ± 3.0	–2,727.0 ± 3.1
		S^0 (J mol^{-1} K^{-1})	S^0 (kJ mol^{-1} K^{-1})
RH	RH	104.2 ± 1.1	110.6 ± 1.2
HP	RH	103.7 ± 1.1	110.2 ± 1.2
SUP	SUP	108.2 ± 1.1	114.7 ± 1.2
		W_H–TW_S (J mol^{-1})	W_H–TW_S (J mol^{-1})
RH	RH	13.6 ± 0.4	–9.1 ± 0.4
HP	RH	13.6 ± 0.4	–9.1 ± 0.4
SUP	SUP	13.6 ± 0.4	–9.1 ± 0.4
		d_fG^0 (kJ mol^{-1})	d_fG^0 (kJ mol^{-1})
RH	RH	–2,595.4 ± 2.8	–2,590.3 ± 2.8
HP	RH	–2,595.8 ± 1.8	–2,590.8 ± 1.8
SUP94	SUP94	–2,594.3 ± 3.0	–2,589.3 ± 3.0
SUP98	SUP98	–2,587.0 ± 3.0	–2,581.9 ± 3.0

References

Aksyuk AM, Zhukovskaya TN (1994) Experimental calibration of the phlogopite fluorimeter at 500–700 °C and 1–4 kbar, and estimated HF concentrations of fluids associated with marble: some examples. Geochim Cosmochim Acta 58:4305–4315

Angel RJ, Kunz M, Miletich R, Woodland AB, Koch M, Xirouchakis D (1999) High-pressure phase transition in $CaTiOSiO_4$ titanite. Phase Trans 68(3B):533–543

Barton MD (1982) The thermodynamic properties of topaz solid solutions and some petrological applications. Am Mineral 67:956–974

Berman RG (1988) Internally-consistent thermodynamic data for minerals in the system Na_2O–K_2O–CaO–MgO–FeO–Fe_2O_3–Al_2O_3–SiO_2–TiO_2–H_2O–CO_2. J Petrol 29:445–522

Berman RG (1990) Mixing properties of Ca–Mg–Fe–Mn garnets. Am Mineral 75:328–344

Berman RG, Brown TH (1985) Heat capacity of minerals in the system Na_2O–K_2O–CaO–MgO–FeO–Fe_2O_3–Al_2O_3–SiO_2–TiO_2–H_2O–CO_2: representation, estimation, and high temperature extrapolation. Contrib Mineral Petrol 89:168–183

Bernau R, Franz G (1987) Crystal chemistry and genesis of Nb-, V-, and Al-rich metamorphic titanite from Egypt and Greece. Can Mineral 25:695–705

Birch F (1966) Compressibility; elastic constants. In: Clark SPJ (ed) Handbook of physical constants. Geological Society of America, New York

Birch WD (1983) Babingtonite, fluorapophyllite and sphene from Harcourt, Victoria, Australia. Mineral Mag 47:377–380

Boettcher AL (1970) The system CaO–Al_2O_3–SiO_2–H_2O at high pressures and temperatures. J Petrol 11:337–379

Bohlen SR, Essene EJ (1978) The significance of metamorphic fluorite in the Adirondacks. Geochim Cosmochim Acta 42:1669–1678

Boles JR, Coombs DS (1977) Zeolite facies alteration of sandstones in the Southland syncline, New Zealand. Am J Sci 277:982–1012

Carmichael RS (1984) CRC handbook of physical properties of rocks. CRC Press, Boca Raton

Carswell DA, Wilson RN, Zhai M (1996) Ultra-high pressure aluminous titanites in carbonate-bearing eclogites at Shuanghe in Dabieshan, Central China. Mineral Mag 60:461–471

Chatterjee ND, Johannes W, Leistner H (1984) The system CaO–Al_2O_3–SiO_2–H_2O: new phase equilibria data, some calculated phase relations, and their petrological applications. Contrib Mineral Petrol 88:1–13

Chrosch J, Bismayer U, Salje EKH (1997) Anti-phase boundaries and phase transitions in titanite: an X-ray diffraction study. Am Mineral 82:677–681

Davies PK, Navrotsky A (1981) Thermodynamics of solid solution formation in NiO–MgO and NiO–ZnO. J Solid State Chem 38:264–276

Davies PK, Navrotsky A (1983) Quantitative correlations of deviations from ideality in binary and pseudo-binary solid solutions. J Solid State Chem 46:1–22

Dawson JB, Smith JV, Steele IM (1994) Trace-element distribution between coexisting perovskite, apatite and titanite from Oldoinyo Lengai, Tanzania. Chem Geol 117:285–290

Deer WA, Howie RA Zussman J (1992) An introduction to the rock-forming minerals, no 696. Longman Scientific and Technical, Hong Kong

Delany JM, Helgeson HC (1978) Calculation of the thermodynamic consequences of dehydration in subducting oceanic crust to 100 kb and > 800 °C. Am J Sci 278:638–686

Droll K, Seck HA (1984) A new sampling technique for fluid phases in hydrothermal experiments applied to the determination of the HF-fugacities of the WFQ-buffer. Contrib Mineral Petrol 88:276–279

Enami M, Suzuki K, Liou JG, Bird DK (1993) Al–Fe^{3+} and F–OH substitutions in titanite and constraints on their P–T dependence. Eur J Mineral 5:219–231

Essene EJ, Bohlen SR (1985) New garnet barometers in the system CaO–FeO–Al_2O_3–SiO_2–TiO_2 (CFAST). EOS Trans Abstr 66:386

Evans BW, Patrick BE (1987) Phengite-3T in high-pressure metamorphosed granitic orthogneisses, Seward Peninsula, Alaska. Can Mineral 25:141–158

Franz G (1987) Breakdown of amphibole and the formation of Al-titanite – an example from the polymetamorphic 'Chephren-Diorite' (Gebl el Asr, SW Egypt). Publication Occasionelle, Centre International pour la formation et les échanges géologiques, Paris, 14th Colloquium African Geology, TU Berlin

Franz G, Spear FS (1983) High pressure metamorphism of siliceous dolomites from the central Tauern Window, Austria. Am J Sci 283:396–413

Franz G, Spear FS (1985) Aluminous titanite (sphene) from the Eclogite Zone, south-central Tauern Window, Austria. Chem Geol 50:33–46

Frost BR, Camberlain KR, Schumacher JC (2001) Sphene (titanite): phase relations and role as a geochronometer. Chem Geol 172:131–148

Fyfe WS, Turner FJ, Verhoogen, J (1958) Metamorphic reactions and metamorphic facies. Geol Soc Am Mem 73:259

Ghent ED, Stout MZ (1994) Geobarometry of low-temperature eclogites: applications of isothermal pressure-activity calculations. Contrib Mineral Petrol 116:500–507

Ghose S, Yoshiaki I, Hatch DM (1991) Paraelectric–antiferroelectric phase transition in titanite, $CaTiSiO_5$. I. A high temperature X-ray diffraction study of the order parameter and transition mechanism. Phys Chem Mineral 17:591–603

Gibert F, Moine B, Gibert P (1990) Aluminous titanite (sphene) crystallised under low/medium pressure in the calc-silicate gneisses of the Montagne Noire. Comptes Rendus Acad Sci, Serie II, t. 311:657–663

Gittins J, Tuttle OF (1964) The system CaF_2–$Ca(OH)_2$–$CaCO_3$. Am J Sci 262:66–75

Gopal ESR (1966) Specific heats at low temperatures. Heywood Books, London

Grapes R, Watanabe T (1992) Paragenesis of titanite in metagreywackes of the Franz Josef–Fox Glacier area, Southern Alps, New Zealand. Eur J Mineral 4:547–555

Green TH, Pearson NJ (1986) Ti-rich accessory phase saturation in hydrous mafic-felsic compositions at high P,T. Chem Geol 54:185–201

Haas JL Jr, Fisher JR (1976) Simultaneous evaluation and correlation of thermodynamic data. Am J Sci 276:525–545

Hammer VMF, Beran A, Endisch D, Rauch F (1996) OH concentrations in natural titanites determined by FTIR spectroscopy and nuclear reaction analysis. Eur J Mineral 8:281–288

Haselton HTJ, Cygan GL, D'Angelo WM (1988) Chemistry of aqueous solutions coexisting with fluoride buffers in the system K_2O–Al_2O_3–SiO_2–H_2O–F_2O (1 kbar, 400–700 °C). Econ Geol 83:163–173

Hellman PL, Green TH (1979) The role of sphene as an accessory phase in high-pressure partial melting of hydrous mafic compositions. Earth Planet Sci Lett 42:191–201

Hirajima T, Zhang R, Li J, Cong B (1992) Petrology of the nyböite-bearing eclogite in the Donghai area, Jiangsu Province, eastern China. Mineral Mag 56:37–46

Holland TJB (1979) High water activities in the generation of high pressure kyanite eclogites of the Tauern Window. J Geol 87:1–27

Holland TJB (1983) The experimental determination of activities in disordered and short-range ordered jadeitic pyroxenes. Contrib Mineral Petrol 82:214–220

Holland TJB (1989) Dependence of entropy on volume for silicate and oxide minerals: a review and a predictive model. Am Mineral 74:5–13

Holland TJB, Powell R (1998) An internally consistent thermodynamic data set for phases of petrological interest. J Metamorph Geol 16:309–343

Hughes JM, Bloodaxe ES, Hanchar JM, Foord EE (1997) Incorporation of rare earth elements in titanite: stabilization of the A2/a dimorph by creation of antiphase boundaries. Am Mineral 82:512–516

Hunt JA, Kerrick DM (1977) The stability of sphene: experimental re-determination and geologic implications. Geochim Cosmochim Acta 41:279–288

Itaya T, Brothers RN, Black PM (1985) Sulfides, oxides and sphene in high-pressure schist from New Caledonia. Contrib Mineral Petrol 91:151–162

Izumi F (1993) Rietveld analysis programs RIETAN and PREMOS and special applications. In Young RA (ed) The Rietveld method. Oxford University Press, Oxford, pp 236–253

Jacobs GK, Kerrick DM (1981) Devolatilization equilibria in H_2O–CO_2 and H_2O–CO_2–NaCl fluids: an experimental and thermodynamic evaluation at elevated pressures and temperatures. Am Mineral 66:1135–1153

Johnson JW, Oelkers RH, Helgeson HC (1991) SUPCRT92: a software package for calculating the standard molal thermodynamic properties of minerals, gases, aqueous species, and reactions from 1 to 5,000 bars and 0° to 1,000 °C. Short course manual presented at the Annual Meeting of the Geol Soc Am 1991, p 151

Kek S, Aroyo M, Bismayer U, Schmidt C, Eichhorn K, Krane HG (1997) The two-step phase transition of titanite, $CaTiSiO_5$: a synchrotron radiation study. Z Kristallogr 212:9–19

Kerrick DM, Jacobs GK (1981) A modified Redlich-Kwong equation for H_2O, CO_2, and H_2O-CO_2 mixtures at elevated pressures and temperatures. Am J Sci 281:735–767

Kim Y-I, Izumi F (1994) Structure refinement with a new version of the Rietveld-refinement program RIETAN. J Ceram Soc Jpn 102:401–404

Kowallis BJ, Christiansen EH, Griffin DT (1997) Compositional variations in titanite. Geol Soc Am Annu Meeting Abstr Program 29(6):402

Krogh EJ, Andresen A, Bryhni I, Broks TM, Kristensen SE (1990) Eclogites and polyphase P–T cycling in the Caledonian Uppermost Allochthon in Troms, northern Norway. J Metamorph Geol 8:289–309

Leonard BF, Buddington AF (1964) Ore deposits of the St. Lawrence Co. Magnetite district, NW Adirondacks, NY. US Geol Surv Prof Pap 377:1–259

López Sánchez-Vizcaíno V, Connolly JAD, Gómez-Pugnaire MT (1997) Metamorphism and phase relations in carbonate rocks from the Nevado–Filábride Complex (Cordilleras Béticas, Spain): applications of the Ttn + Rt + Cal + Qtz + Gr buffer. Contrib Mineral Petrol 126:292–302

Maier CG, Kelley KK (1932) An equation for the representation of high temperature heat content data. J Am Chem Soc 54:3243–3246

Makanjuola AA, Howie RA (1972) The mineralogy of the glaucophane schists and associated rocks from Ile de Groix, Brittany, France. Contrib Mineral Petrol 35:83–118

Manning CE, Bohlen SR (1991) The reaction titanite + kyanite = anorthite + rutile and titanite–rutile barometry in eclogites. Contrib Mineral Petrol 109:1–9

Markl G, Piazolo S (1999) Stability of high-Al titanite from low-pressure calcsilicates in light of fluid and host-rock composition. Am Mineral 84:37–47

Meyer H-W, Bismayer U, Adiwidjaja G, Zhang M, Nistor L, Van Tendeloo G (1998) Natural titanite and malayaite: structural investigations and the 500 K anomaly. Phase Trans 67:27–49

Miller AR (1981) BASIC programs for scientists and engineers. SYBEX Inc, Berkeley

Mukhopadhyay A, Bhattacharya A, Mohanty L (1992) Geobarometers involving clinopyroxene, garnet, plagioclase, ilmenite, rutile, sphene and quartz: estimation of pressure in quartz-absent assemblages. Contrib Mineral Petrol 110:346–354

Munoz JL, Eugster HP (1969) Experimental control of fluorine reactions in hydrothermal systems. Am Mineral 54:943–959

Newton RC, Wood BJ (1980) Volume behavior of silicate solid solutions. Am Mineral 65:733–745

Oberti R, Smith DC, Rossi G, Caucia F (1991) The crystal-chemistry of high-aluminium titanites. Eur J Mineral 3:777–792

Paterson BA, Stephens WE (1992) Kinetically induced compositional zoning in titanite: implications for accessory-phase/melt

partitioning of trace elements. Contrib Mineral Petrol 109:373–385
Perkins D, Westrum EF Jr, Essene EJ (1980) The thermodynamic properties and phase relations of some minerals in the system $CaO–Al_2O_3–SiO_2–H_2O$. Geochim Cosmochim Acta 44:61–84
Poirier JP (1991) Introduction to the physics of the Earth's interior. Cambridge University Press, Cambridge
Powell R (1978) Equilibrium thermodynamics in petrology. Harper and Row, London
Pownceby MI, O'Neill HSC (1994) Thermodynamic data from redox reactions at high temperatures. III. Activity–composition relations in Ni–Pd alloys from EMF measurements at 850–1,250 K, and calibration of the NiO + Ni–Pd assemblage as a redox sensor. Contrib Mineral Petrol 116:327–339
Price JD, Hogan JP, Gilbert MC, Morgan MGB IV (1999) Experimental study of titanite–fluorite equilibria in the A-type Mount Scott Granite: implications for assessing F contents of felsic magma. Geology 27(10):951–954
Rice JM (1980) Phase equilibria involving humite minerals in impure limestones, Part I. Calculated stability of clinohumite. Contrib Mineral Petrol 71:219–235
Robie RA, Hemingway BS (1995) Thermodynamic properties of minerals and related substances at 298.15 K and 1 bar (10^5 pascals) pressure and at higher higher temperatures. US Geol Soc Survey Bull 2131
Sahama TG (1946) On the chemistry of the mineral titanite. C R Soc Geol Finlande 19(138):88–120
Salje E, Schmidt C, Bismayer U (1993) Structural phase transition in titanite, $CaTiSiO_5$: a raman spectroscopic Study. Phys Chem Mineral 19:502–506
Schreyer W (1988) Experimental studies on metamorphism of crustal rocks under mantle pressures. Mineral Mag 52:1–26
Smith DC (1980) Highly aluminous sphene (titanite) in natural high-pressure hydrous-eclogite-facies rocks from Norway and Italy, and in experimental runs at high pressure. 26th Int Geol Congress, Paris, France (Abstr), Section 02.3.1:145
Smith DC (1981) The pressure and temperature dependence of Al-solubility in sphene in the system Ti–Al–Ca–Si–O–F. Prog Exp Petrol Natl Env Res Council Publication Series D-18, UK, pp 193–197
Sobolev NV, Shatsky VS (1990) Diamond inclusions in garnets from metamorphic rocks: a new environment for diamond formation. Nature 343:742–746
Spear FS (1981) An experimental study of hornblende stability and compositional variability in amphibolite. Am J Sci 281:697–734
Speer JA, Gibbs GV (1976) The crystal structure of synthetic titanite $CaTiOSiO_4$, and the domain textures of natural titanites. Am Mineral 61:238–247
Taylor M, Brown GE (1976) High-temperature structural study of the $P2_1/a <-> A2/a$ phase transition in synthetic titanite, $CaTiSiO_5$. Am Mineral 61:435–447
Thiéblot L, Téqui C, Richet P (1999) High-temperature heat capacity of grossular ($Ca_2Al_2Si_3O_{12}$), enstatite ($MgSiO_3$) and titanite ($CaTiSiO_5$). Am Mineral 84:848–855
Thompson AB, Ellis DJ (1994) CaO + MgO + Al_2O_3 + SiO_2 + H_2O to 35 KB: amphibole, talc, and zoisite dehydration and melting reactions in the silica-excess part of the system and their possible significance in subduction zones, amphibolite melting, and magma fractionation. Am J Sci 294:1229–1289
Tribuzio R, Messiga B, Vannucci R, Bottazzi P (1996) Rare earth element redistribution during high-pressure-low-temperature metamorphism in ophiolitic Fe-gabbros (Liguria, northwestern Italy): implications for light REE mobility in subduction zones. Geology 24(8):711–714
Troitzsch U (2000) The crystal structure and thermodynamic properties of titanite solid-solution $Ca(Ti,Al)(O,F)SiO_4$. PhD Thesis, Australian National University, Canberra
Troitzsch U, Ellis DJ (1999) The synthesis and crystal structure of $CaAlFSiO_4$, the Al–F analog of titanite. Am Mineral 84:1162–1169
Troitzsch U, Ellis DJ, Thompson J, FitzGerald JD (1999) Crystal structural changes in titanite along the join TiO–AlF. Eur J Mineral 6:955–965
Tropper P, Manning CE, Essene EJ (1999) The synthesis and stability of Al–F-rich titanites between 900 and 1,100 °C and 11 to 40 kbar. Berichte Deutsch Mineralog Ges 1:230
Tropper P, Manning C, Essene E (2000) Activity-composition relations of titanite in the system $CaTiSiO_4O–CaAlSiO_4F$ at 1,000–1,100 °C. J Conf Abstr 5(1):104
Valley JW, Essene EJ (1980) Calc-silicate reactions in Adirondack marbles: the role of fluids and solid solutions: summary. Geol Soc Am Bull 91(1):114–117
Valley JW, Petersen EU, Essene EJ, Bowman JR (1982) Fluorphlogopite and fluortremolite in Adirondack marbles and calculated C–O–H–F fluid compositions. Am Mineral 67:545–557
Van Heurck C, Van Tendeloo G, Ghose S, Amelinckx S (1991) Paraelectric–antiferroelectric phase transition in titanite, $CaTiSiO_5$. II. Electron diffraction and electron microscopic studies of the transition dynamics. Phys Chem Mineral 17:604–610
Webster LD, Holloway JR (1990) Partitioning of F and Cl between magmatic hydrothermal fluids and highly evolved granitic magmas. In Stein HJ, Hannah JL (eds) Ore-bearing granite systems; Petrogenesis and mineralising processes. Geol Soc Am Spec Pap 246:21–34
Wones DR (1989) Significance of the assemblage titanite + magnetite + quartz in granitic rocks. Am Mineral 74:744–749
Wood BJ, Fraser DG (1978) Elementary thermodynamics for geologists. Oxford University Press, Oxford
Xirouchakis D, Tangeman JA (1998) Thermochemistry of end-member titanite ($CaTiSiO_5$). EOS Trans Abstr 79(45):880
Yau YC, Anovitz LM, Essene EJ, Peacor DR (1984) Phlogopite–chlorite reaction mechanisms and physical conditions during retrograde reactions in the Marble Formation, Franklin, New Jersey. Contrib Mineral Petrol 88:299–306
Ye K, Hirajima T (1996) High-pressure marble at Yangguantun, Rongcheng County, eastern China. Mineral Petrol 57:151–156
Zhang M, Salje EKH, Bismayer U, Unruh H-G, Wruck B, Schmidt C (1995) Phase transition(s) in titanite $CaTiSiO_5$: an infrared spectroscopic, dielectric response and heat capacity study. Phys Chem Mineral 22:41–49